Quantum perspectives in computing, sensing, communication, and metrology

Edoardo Charbon

EPFL

EPFL, Lausanne, Switzerland

Aknowledgements

Simone Frasca
Jiang Gong
Pascal ‘t Hart
Harald Homulle
Yatao Peng
Andrea Ruffino

and

Masoud Babaie
Andrew Dzurak
M. Fernando Gonzalez-Zalba
Daniele Faccio
Fabio Sebastiano

Outline

1. Quantum computing (2 periods)
2. Cryogenic electronics (2 periods)

Available in a future class:

3. Quantum algorithms (2 periods)
4. Quantum imaging and communications (1 period)
5. Quantum metrology (2 periods)

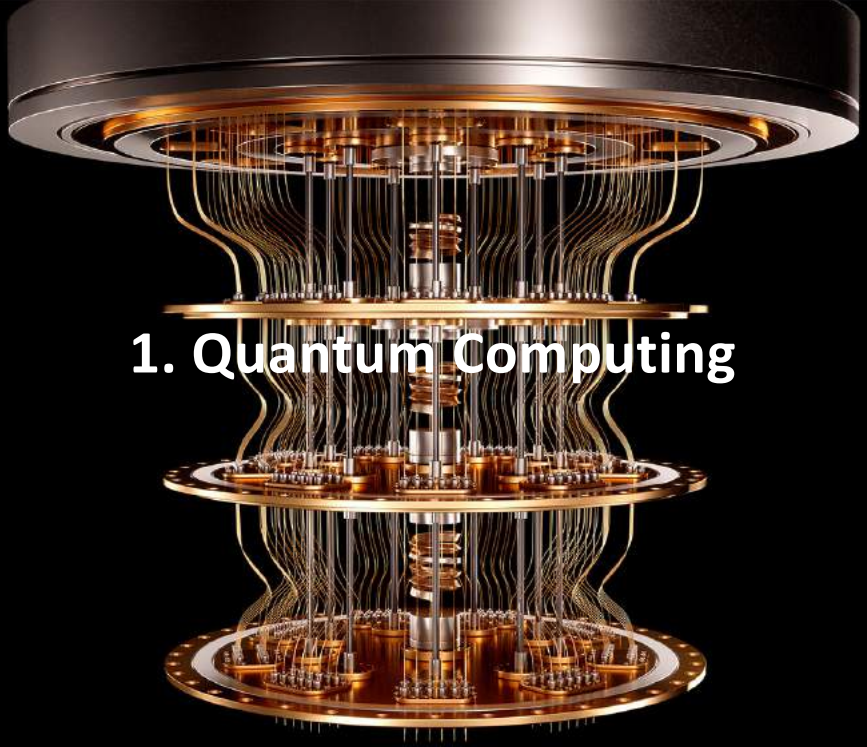

1. Quantum Computing

Suggested Reading

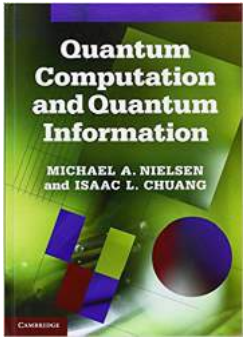

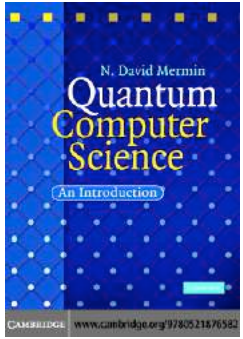

The First Quantum Revolution

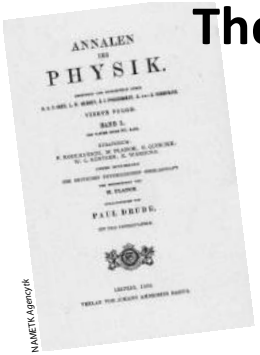

NAMETK Agency/R

Planck Explains Blackbody Radiation (1900)

Einstein Explains Photoelectric Effect (1905)

Bohr's Theory of Atomic Spectra (1913)

Discovery of Superconductivity (1911)

TEXAS CENTER FOR SUPERCONDUCTIVITY, UNIVERSITY OF HOUSTON

Bose-Einstein Condensation Predicted (1924)

Pauli Exclusion Principle (1925)

Schrödinger Equation; Copenhagen Interpretation (1926)

Heisenberg Uncertainty Principle (1927)

Dirac Equation for the Electron (1928)

Anti-Electron Discovered (1932)

Schrödinger's Cat Paper; Einstein-Podolsky-Rosen Paper about Local Realism (1935)

Superfluidity Discovered (1938)

BETTMANN/CORBIS

Atomic Bomb (1945)

Transistor (1947)

AT&T ARCHIVES

Quantum Electrodynamics and Renormalization (1948)

1900s | 1910s | 1920s | 1930s | 1940s

M. Tegmark & J.A. Wheeler, 2001

The First Quantum Revolution

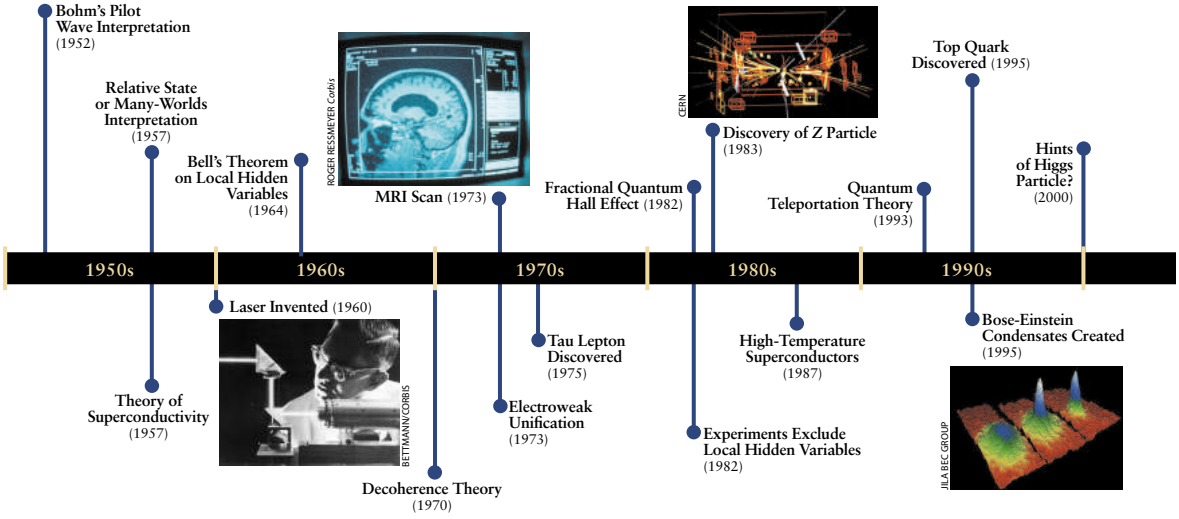

M. Tegmark & J.A. Wheeler, 2001

Weird Quantum Properties: Superposition & Entanglement

Superposition

CLASSICAL UNCERTAINTY

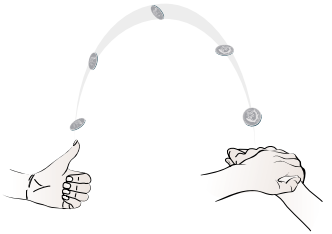

COIN TOSS

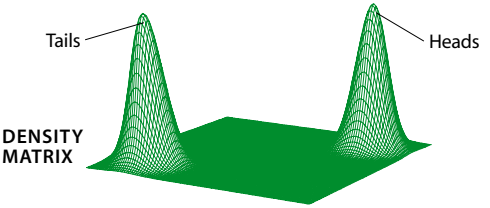

QUANTUM UNCERTAINTY

COHERENT SUPERPOSITION

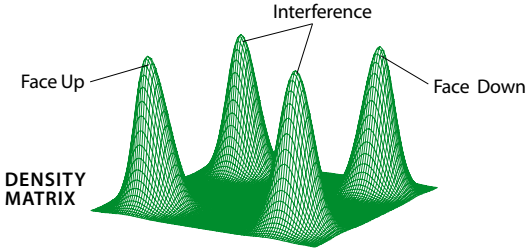

M. Tegmark & J.A. Wheeler, 2001

Coherence / Decoherence

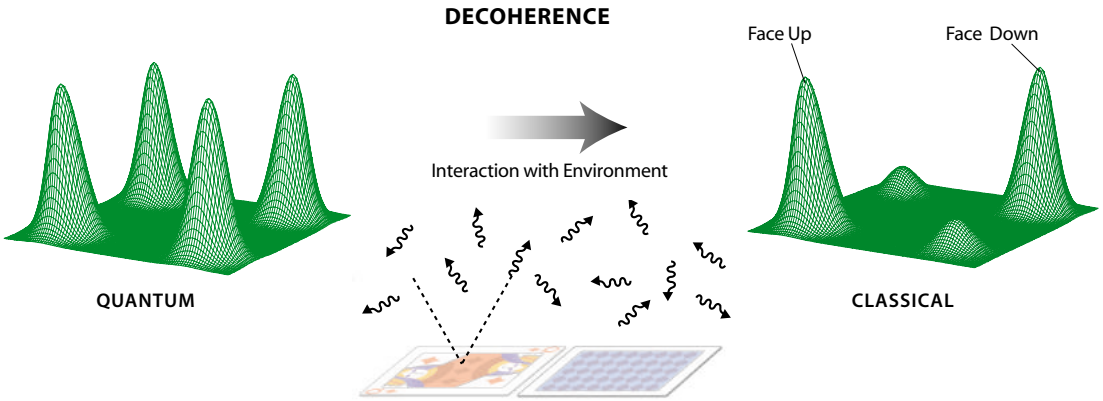

M. Tegmark & J.A. Wheeler, 2001

Entanglement

Definition: two particles are entangled if the quantum state of one particle cannot be described independently from the quantum state of the other particle.

Intuition: measuring the quantum state of one particle implies knowledge of the quantum state (e.g. momentum, spin, polarization, etc.) of the other entangled particle using the same projection.

The Second Quantum Revolution

- Spearheaded by many, *in primis* Richard Feynman
- Proposal to use of **entanglement** and **superposition** for computation
- Fundamentals and theory developed in the 1980-2000s

There is plenty of space at the bottom

- Richard Feynman

The Promise of Quantum Computing

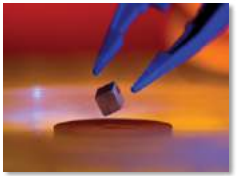

Energy
Room-temperature superconductivity

Health
Quantum chemistry

Internet Security

Source: L. Vandersypen, ISSCC 2017

Quantum Bit (Qubit)

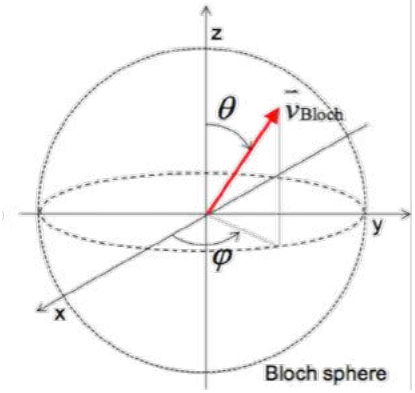

$$|\psi\rangle = \alpha_0 |0\rangle + \alpha_1 |1\rangle$$

- Superposition
- Entanglement

The Power of Superposition

1 qubit.....2 states
2 qubits.....4 states

N qubits.....2^N states

40 qubits: 10^{12} parallel operations
300 qubits: more than the atoms in the universe

State-of-the-Art

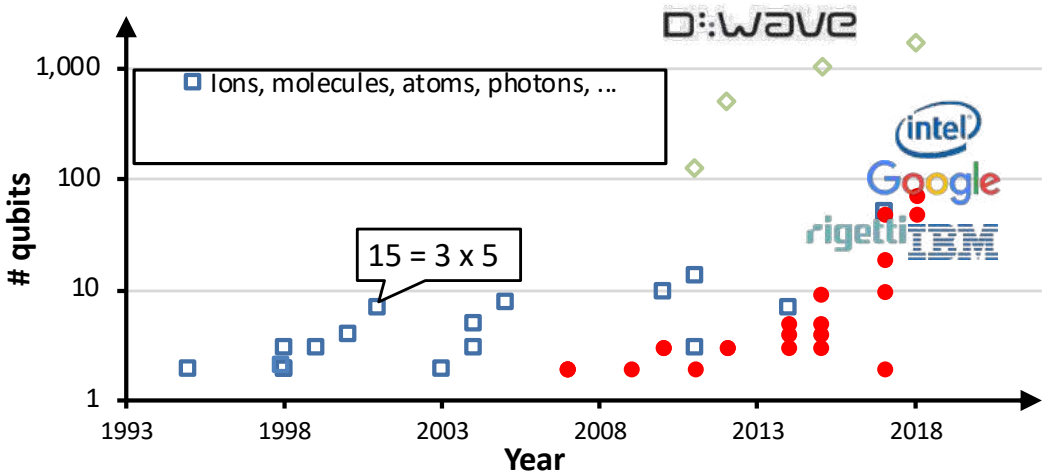

How Far Are We from Something Useful?

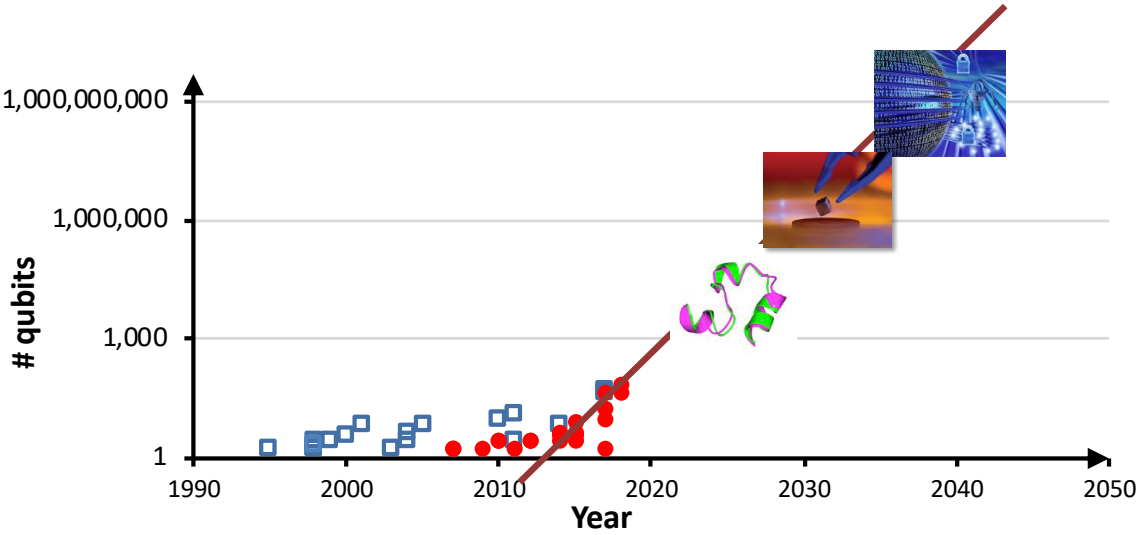

Quantum Supremacy or Quantum Advantage

> Quantum supremacy is the potential ability of quantum computing devices to solve problems that classical computers practically cannot.
>
> [Wikipedia]

Google claims to have reached quantum supremacy (Financial Times)

Report on a an accepted paper to a peer-reviewed publication

Solid-state Qubit Implementations Today

- Based on superconducting qubits
- First multi-qubit chips announced
- Freely available qubits on line

72-qubit chip announced

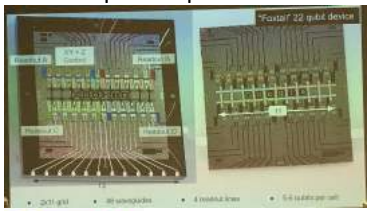

Google

16 Qubits online version

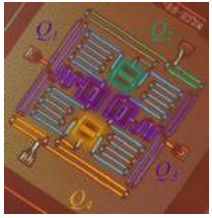

IBM

50 qubit chip announced

49 qubit chip

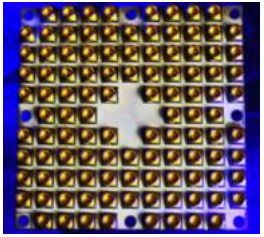

intel

19 qubit chip

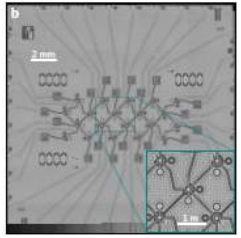

Source: Tristan Meunier

Solid-state Qubit Implementations Today

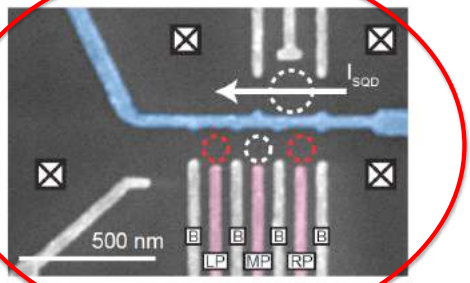

Semiconductor quantum dots

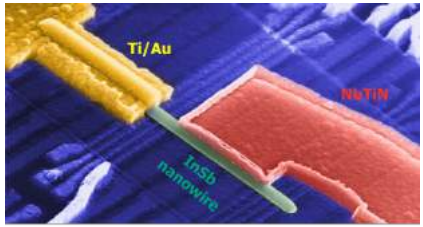

Semiconductor-superconductor hybrids

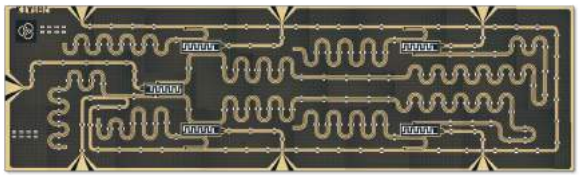

Superconducting circuits

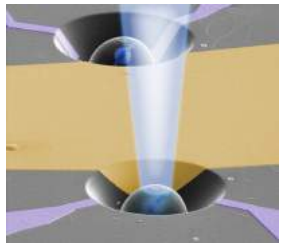

Impurities in diamond or silicon

Source: L. Vandersypen, 2017

Qubits are Fragile

- Environment can cause decoherence due to dephasing and relaxation
- Fidelity

Dephasing

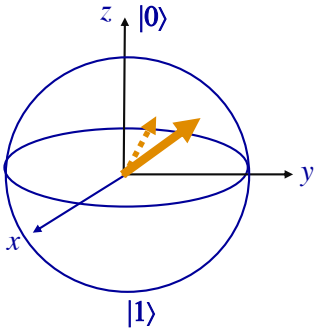

Relaxation

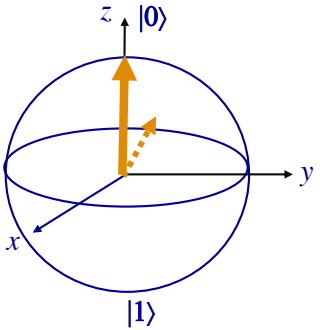

Qubit Transition from |0> to |1>

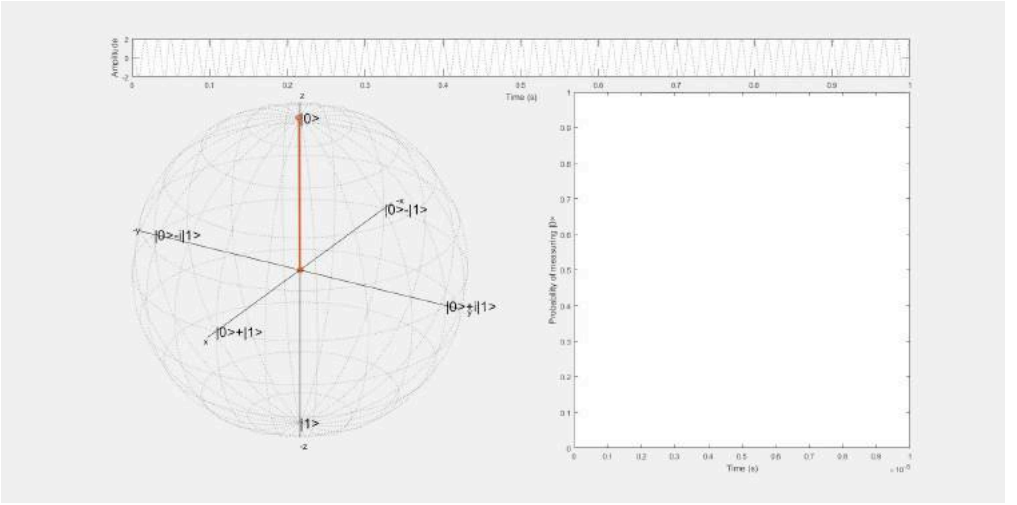

© Jeroen van Dijk

Interfacing Qubits with Classical World

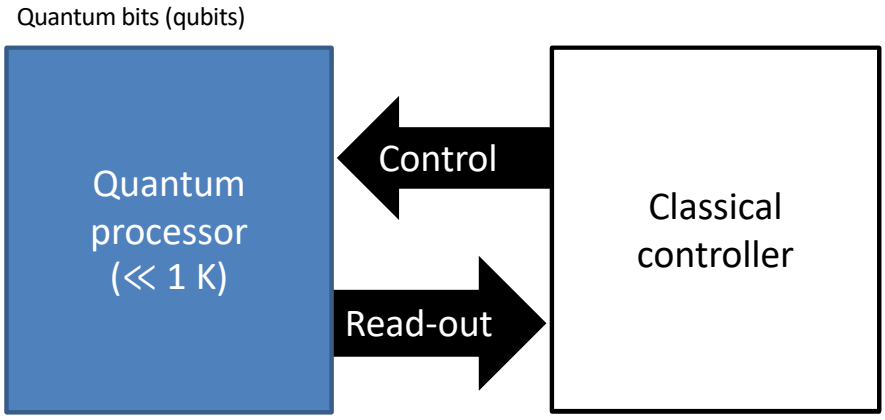

- Carrier frequency: 100 MHz – 15 GHz, 70 GHz
- Pulses: 10 – 100 ns

Interfacing Qubits with Classical World

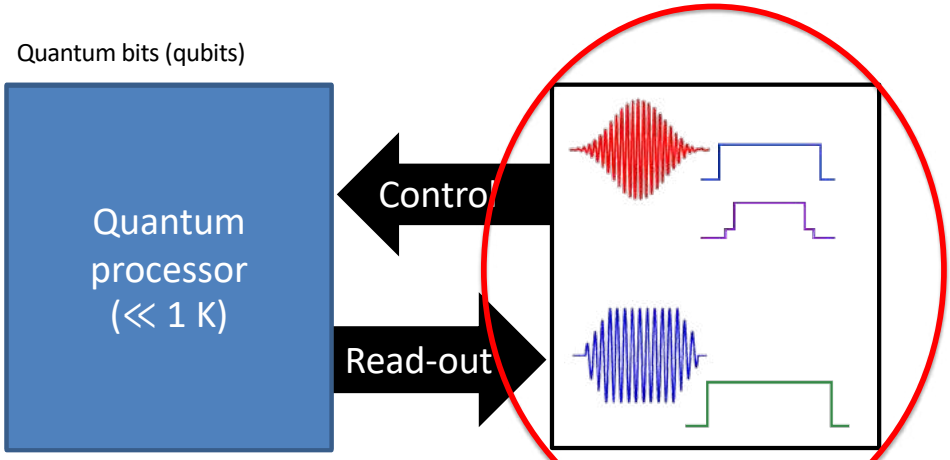

- Carrier frequency: 100 MHz – 15 GHz, 70 GHz
- Pulses: 10 – 100 ns
- Readout techniques for spin qubits: **ESR, EDSR**

ESR: Electron spin resonance – EDSR: Electric dipole spin resonance

Status of Quantum Algorithms

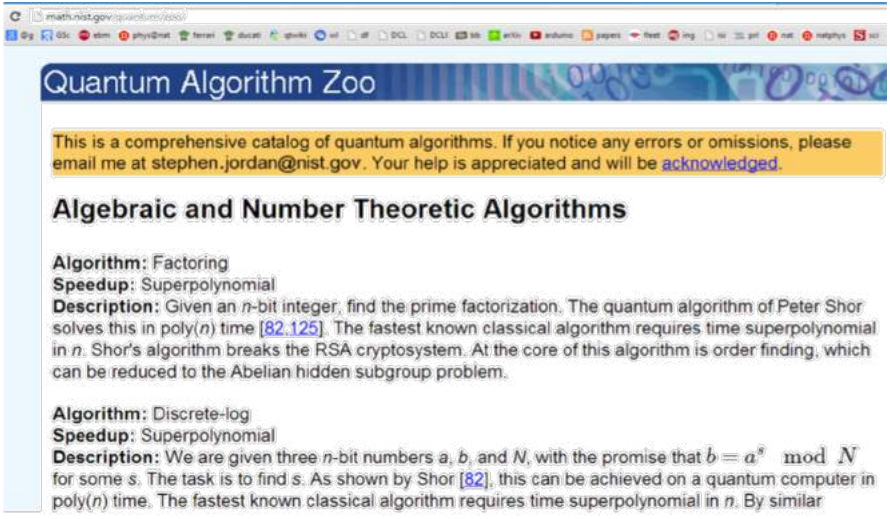

math.nist.gov

Quantum Algorithm Zoo

This is a comprehensive catalog of quantum algorithms. If you notice any errors or omissions, please email me at stephen.jordan@nist.gov. Your help is appreciated and will be acknowledged.

Algebraic and Number Theoretic Algorithms

Algorithm: Factoring
Speedup: Superpolynomial
Description: Given an n-bit integer, find the prime factorization. The quantum algorithm of Peter Shor solves this in poly(n) time [82,125]. The fastest known classical algorithm requires time superpolynomial in n. Shor's algorithm breaks the RSA cryptosystem. At the core of this algorithm is order finding, which can be reduced to the Abelian hidden subgroup problem.

Algorithm: Discrete-log
Speedup: Superpolynomial
Description: We are given three n-bit numbers a, b, and N, with the promise that $b = a^s \mod N$ for some s. The task is to find s. As shown by Shor [82], this can be achieved on a quantum computer in poly(n) time. The fastest known classical algorithm requires time superpolynomial in n. By similar

~50 algorithms with quantum speedup, but most people know 2.

How Many Qubits Do We Need?

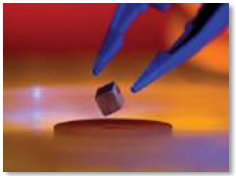

Energy
Room-temperature superconductivity

Perhaps millions?

Health
Quantum chemistry

> 200 logical qubits

Internet Security

> 2000 logical qubits

Quantum Computing Stack

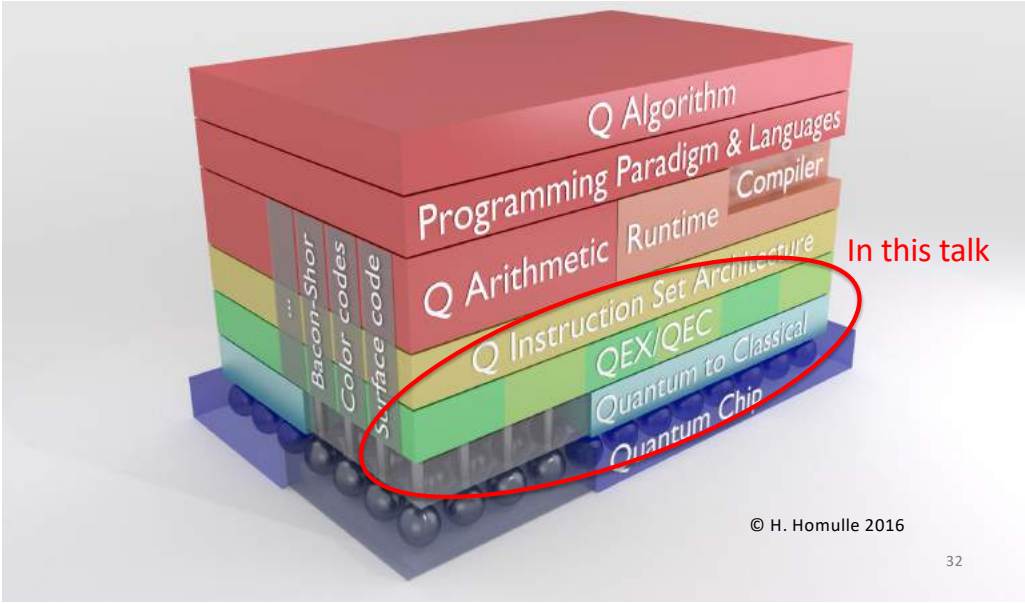

Quantum Computer Architecture

A Real-life Quantum Computer

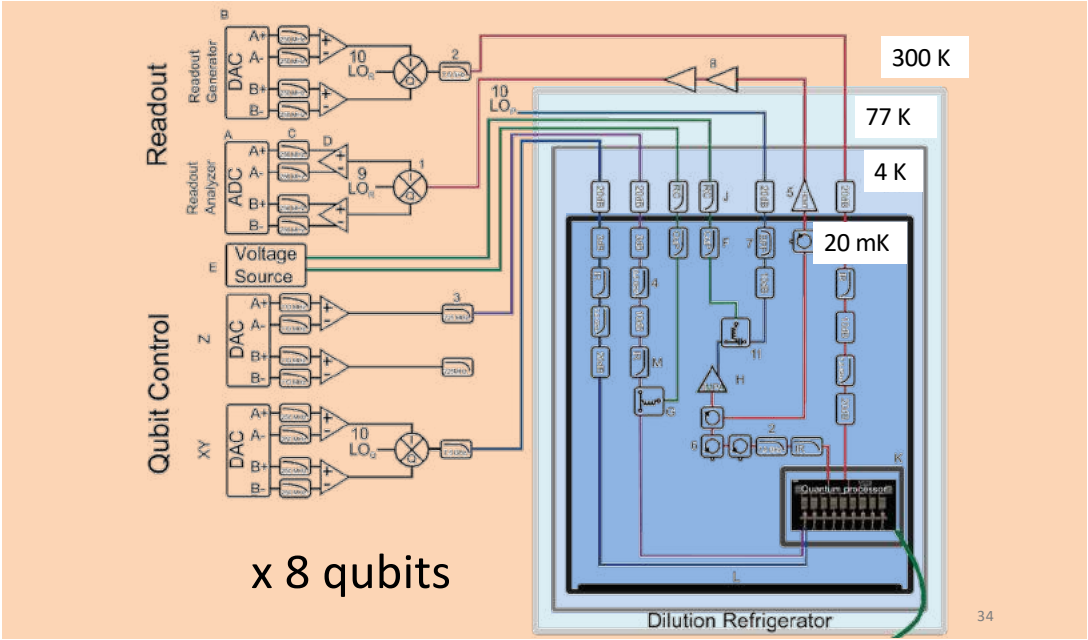

Today's Solution

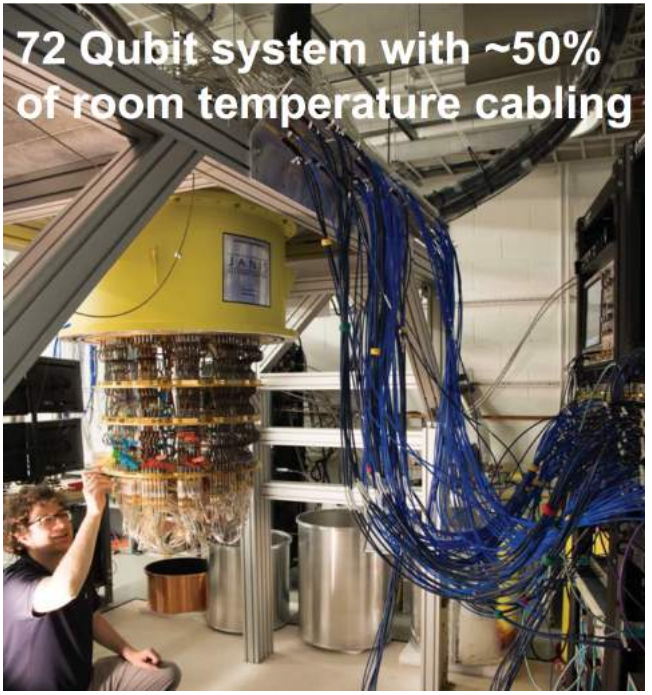

Image: Google Bristlecone. Taken from: J.C. Bardin et al., *"An Introduction to Quantum Computing for RFIC Engineers"*, RFIC Symposium 2019

Proposed Solution

- **Proposed solution**
  - Electronics at 4 K
  - Only connections to 4 K to 20 mK are needed

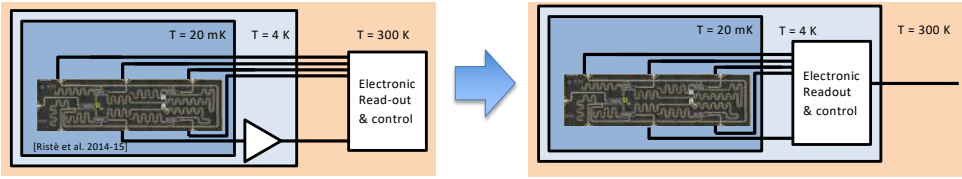

- **Ultimate solution**
  - Qubits at 4 K
  - Monolithic integration

Electronic Readout & Control

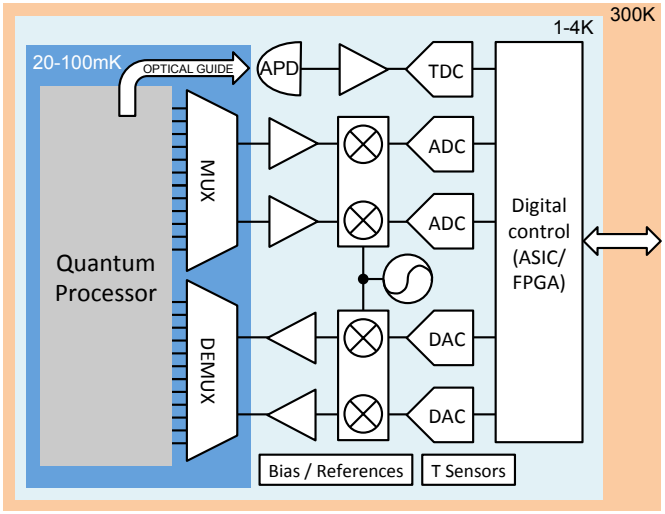

E. Charbon *et al.*, *IEDM* 2016

Cooling Power Issue

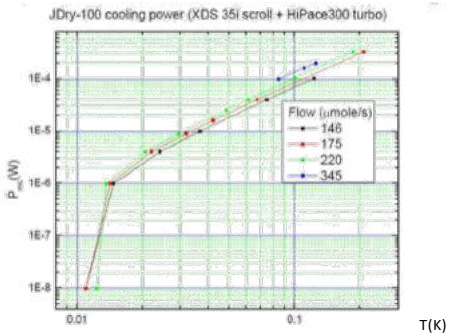

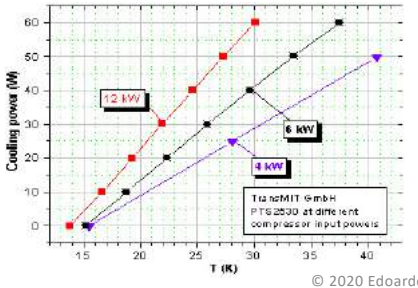

Dilution refrigerator

300 K

70 K

4 K

100 mK

20 mK

Courtesy: Oxford instruments

Scalability Issue

- Noise budget…….< 0.1nV/√Hz
- Power budget (for scalability)……. << 2mW/qubit
- Physical dimensions (for scalability)……. 30nm
- Bandwidth (for multiplexing)……. 1-12GHz
- Kick-back avoidance

2. Cryogenic Electronics

Transistor Modeling at Deep Cryogenic Temperatures

CMOS Modeling: Important Parameters

- MOSFET

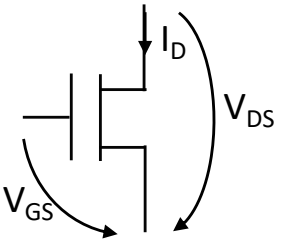

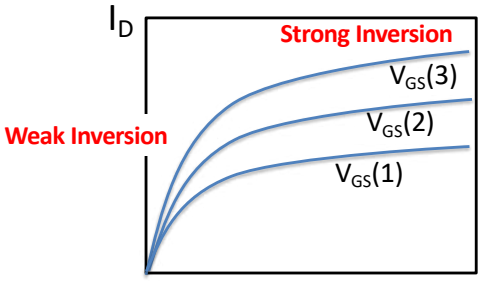

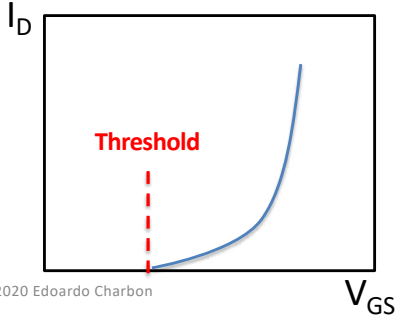

CMOS Modeling: History

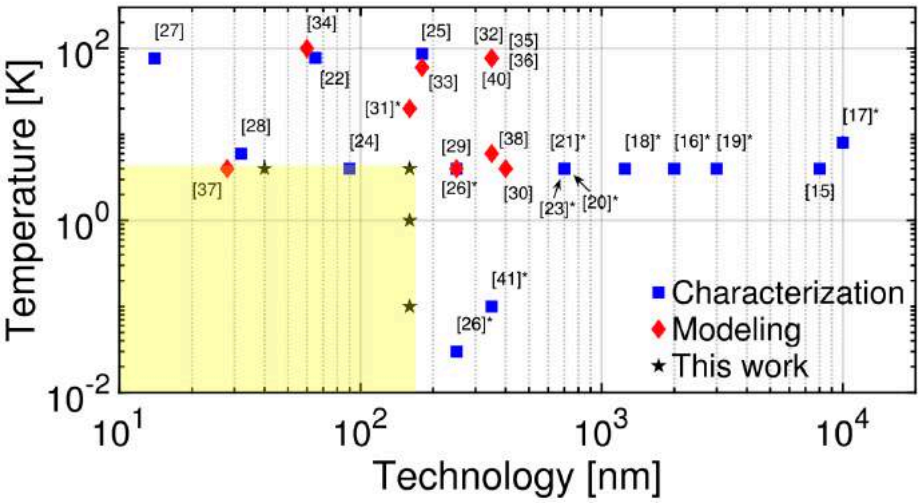

R.M. Incandela et al., *ESSDERC* 2017
R.M. Incandela et al., *J. of EDS 2018*

[16] H. Hanamura *et al.*, "Operation of bulk CMOS devices at very low temperatures," *IEEE J. Solid-State Circuits*, vol. 21, no. 3, pp. 484–490, Jun. 1986, doi: 10.1109/JSSC.1986.1052555.

[17] F. Balestra, L. Audaire, and C. Lucas, "Influence of substrate freeze-out on the characteristics of MOS transistors at very low temperatures," *Solid State Electron.*, vol. 30, no. 3, pp. 321–327, Mar. 1987, doi: 10.1016/0038-1101(87)90190-0.

[18] L. Deferm, E. Simoen, and C. Claeys, "The importance of the internal bulk-source potential on the low temperature kink in NMOSTs," *IEEE Trans. Electron Devices*, vol. 38, no. 6, pp. 1459–1466, Jun. 1991, doi: 10.1109/16.81639.

[19] E. Simoen, B. Dierickx, and C. L. Claeys, "Low-frequency noise behavior of Si NMOSTs stressed at 4.2 K," *IEEE Trans. Electron Devices*, vol. 40, no. 7, pp. 1296–1299, Jul. 1993, doi: 10.1109/16.216435.

[20] E. Simoen and C. Claeys, "Impact of CMOS processing steps on the drain current kink of NMOSFETs at liquid helium temperature," *IEEE Trans. Electron Devices*, vol. 48, no. 6, pp. 1207–1215, Jun. 2001, doi: 10.1109/16.925249.

[21] E. Simoen *et al.*, "Impact of irradiations performed at liquid helium temperatures on the operation of 0.7 μm CMOS devices and read-out circuits," in *Proc. Radiat. Effects Compon. Syst. (RADECS)*, 2003, pp. 369–375.

[22] A. Siligaris *et al.*, "High-frequency and noise performances of 65-nm MOSFET at liquid nitrogen temperature," *IEEE Trans. Electron Devices*, vol. 53, no. 8, pp. 1902–1908, Aug. 2006, doi: 10.1109/TED.2006.877872.

[23] Y. Creten, P. Merken, W. Sansen, R. Mertens, and C. van Hoof, "A cryogenic ADC operating down to 4.2K," in *IEEE Int. Solid-State Circuits Conf. Dig. Tech. Papers*, San Francisco, CA, USA, Feb. 2007, pp. 468–616, doi: 10.1109/ISSCC.2007.373497.

[24] S.-H. Hong *et al.*, "Low-temperature performance of nanoscale MOSFET for deep-space RF applications," *IEEE Electron Device Lett.*, vol. 29, no. 7, pp. 775–777, Jul. 2008, doi: 10.1109/LED.2008.2000614.

[25] G. De Geronimo *et al.*, "Front-end ASIC for a liquid argon TPC," in *Proc. IEEE Nuclear Sci. Symp. Med. Imag. Conf.*, vol. 58. Knoxville, TN, USA, Oct. 2010, pp. 1658–1666, doi: 10.1109/NSSMIC.2010.5874057.

[26] S. R. Ekanayake, T. Lehmann, A. S. Dzurak, R. G. Clark, and A. Brawley, "Characterization of SOS-CMOS FETs at low temperatures for the design of integrated circuits for quantum bit control and readout," *IEEE Trans. Electron Devices*, vol. 57, no. 2, pp. 539–547, Feb. 2010, doi: 10.1109/TED.2009.2037381.

[27] M. Shin *et al.*, "Low temperature characterization of 14nm FDSOI CMOS devices," in *Proc. 11th Int. Workshop Low Temp. Electron. (WOLTE)*, Grenoble, France, Jul. 2014, pp. 29–32, doi: 10.1109/WOLTE.2014.6881018.

[28] A. H. Coskun and J. C. Bardin, "Cryogenic small-signal and noise performance of 32nm SOI CMOS," in *Proc. IEEE MTT-S Int. Microw. Symp. (IMS)*, Tampa, FL, USA, Jun. 2014, pp. 1–4, doi: 10.1109/MWSYM.2014.6848614.

[29] Y. Feng, P. Zhou, H. Liu, J. Sun, and T. Jiang, "Characterization and modelling of MOSFET operating at cryogenic temperature for hybrid superconductor-CMOS circuits," *Semicond. Sci. Technol.*, vol. 19, no. 12, pp. 1381–1385, Oct. 2004, doi: 10.1088/0268-1242/19/12/009.

[30] A. Akturk *et al.*, "Impact ionization and freeze-out model for simulation of low gate bias kink effect in SOI-MOSFETs operating at liquid He temperature," in *Proc. Conf. Simulat. Semicond. Process. Devices (SISPAD)*, Sep. 2009, pp. 1–4, doi: 10.1109/SISPAD.2009.5290227.

[31] A. Akturk *et al.*, "Compact and distributed modeling of cryogenic bulk MOSFET operation," *IEEE Trans. Electron Devices*, vol. 57, no. 6, pp. 1334–1342, Jun. 2010, doi: 10.1109/TED.2010.2046458.

[32] Z. Zhu *et al.*, "Design applications of compact MOSFET model for extended temperature range (60–400 K)," *Electron. Lett.*, vol. 47, no. 2, pp. 141–142, Jan. 2011, doi: 10.1049/el.2010.3468.

[33] P. Martin, A. S. Royet, F. Guellec, and G. Ghibaudo, "MOSFET modeling for design of ultra-high performance infrared CMOS imagers working at cryogenic temperatures: Case of an analog/digital 0.18 μm CMOS process," *Solid-State Electron.*, vol. 62, no. 1, pp. 115–122, 2011, doi: 10.1016/j.sse.2011.01.004.

[34] Z. Chen, H. Wong, Y. Han, S. Dong, and B. L. Yang, "Temperature dependences of threshold voltage and drain-induced barrier lowering in 60 nm gate length MOS transistors," *Microelectron. Rel.*, vol. 54, nos. 6–7, pp. 1109–1114, Jun./Jul. 2014, doi: 10.1016/j.microrel.2013.12.005.

[35] H. Zhao and X. Liu, "Modeling of a standard 0.35 μm CMOS technology operating from 77K to 300K," *Cryogenics*, vol. 59, pp. 49–59, Jan. 2014, doi: 10.1016/j.cryogenics.2013.10.003.

[36] G. S. Fonseca, L. B. de Sá, and A. C. Mesquita, "Extraction of static parameters to extend the EKV model to cryogenic temperatures," in *Proc. SPIE Defense Security*, Baltimore, MD, USA, May 2016, Art. no. 98192B, doi: 10.1117/12.2219734.

[37] A. Beckers *et al.*, "Cryogenic characterization of 28 nm bulk CMOS technology for quantum computing," in *Proc. 47th Eur. Solid-State Device Res. Conf. (ESSDERC)*, Leuven, Belgium, Sep. 2017, pp. 62–65, doi: 10.1109/ESSDERC.2017.8066592.

[38] N. C. Dao *et al.*, "An enhanced MOSFET threshold voltage model for the 6–300 K temperature range," *Microelectron. Rel.*, vol. 69, pp. 36–39, Feb. 2017, doi: 10.1016/j.microrel.2016.12.007.

[39] R. M. Incandela *et al.*, "Nanometer CMOS characterization and compact modeling at deep-cryogenic temperatures," in *Proc. 47th Eur. Solid-State Device Res. Conf. (ESSDERC)*, Leuven, Belgium, Sep. 2017, pp. 58–61, doi: 10.1109/ESSDERC.2017.8066591.

[40] L. Varizat, G. Sou, M. Mansour, D. Alison, and A. Rhouni, "A low temperature 0.35μm CMOS technology BSIM3.3 model for space instrumentation: Application to a voltage reference design," in *Proc. IEEE Int. Workshop Metrol. AeroSpace (MetroAeroSpace)*, Padua, Italy, Jun. 2017, pp. 74–78, doi: 10.1109/MetroAeroSpace.2017.7999541.

[41] A. Rhouni *et al.*, "First-ever test and characterization of the AMS standard bulk 0.35 μm CMOS technology at sub-Kelvin temperatures," *J. Phys. Conf. Series*, vol. 834, no. 1, May 2017, Art. no. 012005, doi: 10.1088/1742-6596/834/1/012005.

R.M. Incandela et al., *J. of EDS 2018*

What Happens to CMOS at Cryo?

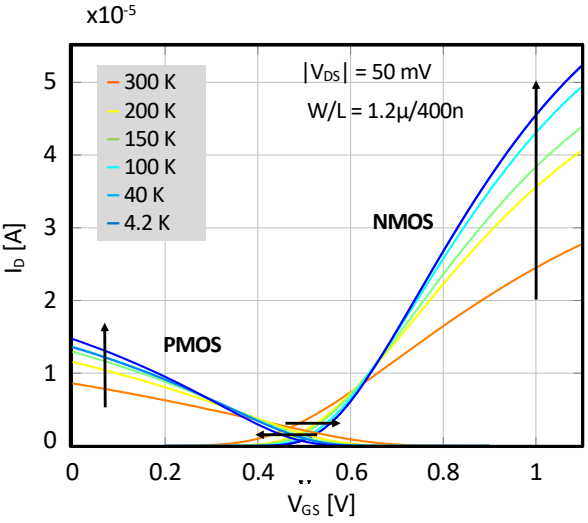

- Threshold voltage increases significantly
- A current kink may appear
- Mismatch in passives and actives is more prominent
- The substrate becomes practically floating
- *The SS is higher but it saturates around 1K*
- Leakage drastically reduces

R.M. Incandela et al., *ESSDERC* 2017
R.M. Incandela et al., *J. of EDS 2018*

How to Characterize MOS Transistors?

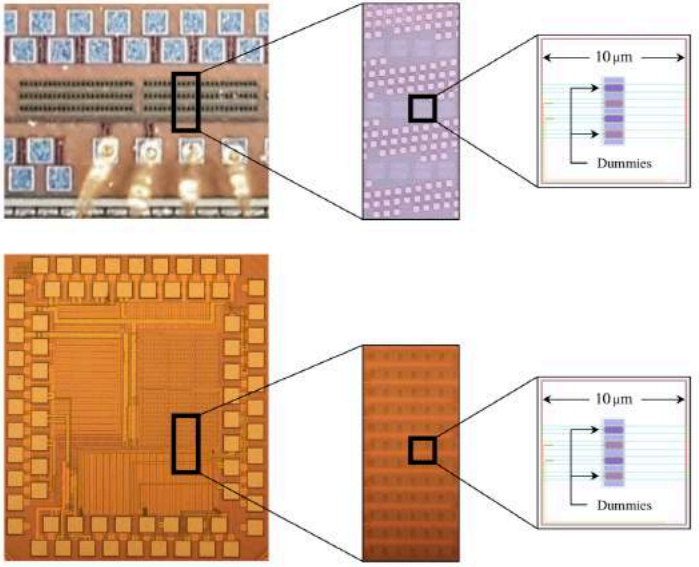

P. 't Hart et al., *J. EDS* 2020

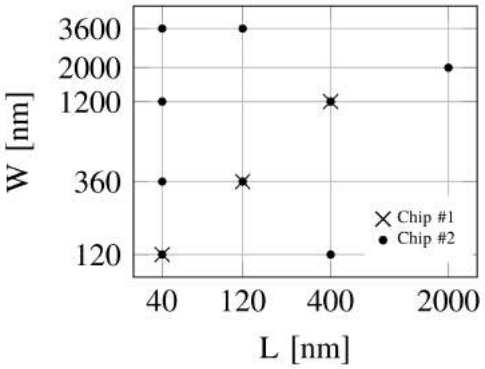

CMOS Characterization in Practice

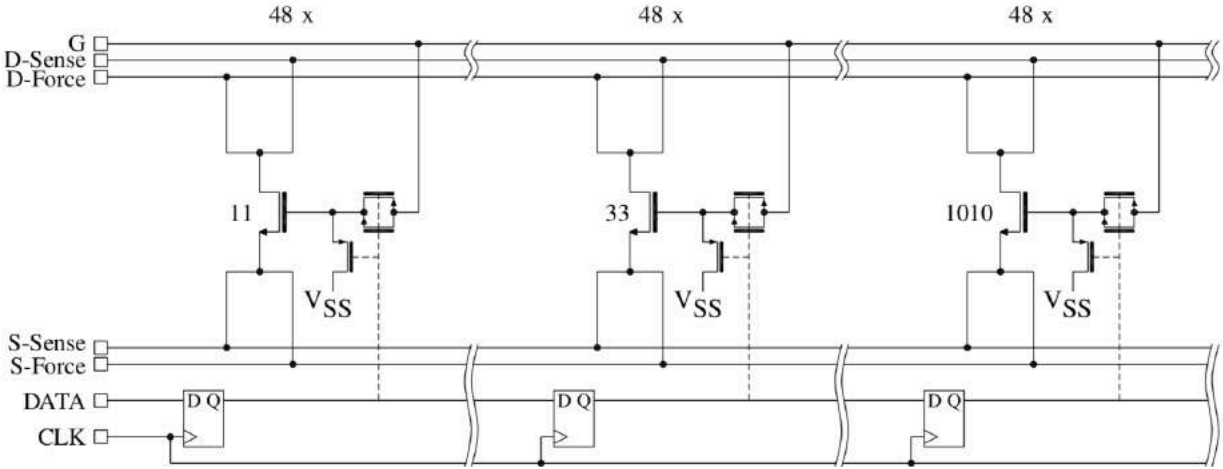

P. 't Hart et al., *J. EDS* 2020

I_D-V_{DS} Characterization (0.16µm)

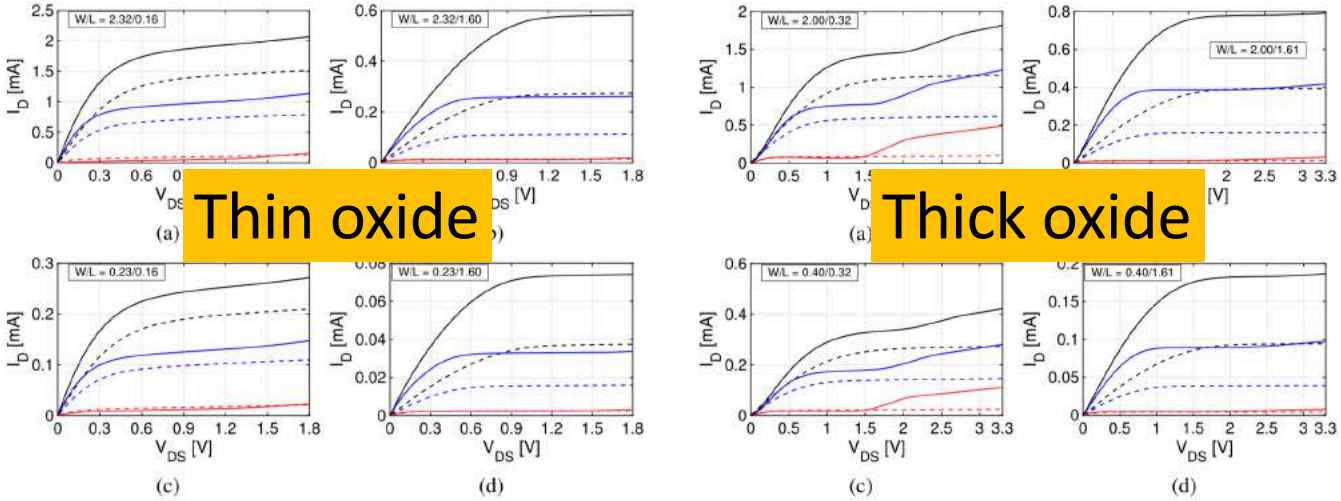

V_{GS} = [0.68 V; 1.24 V; 1.8 V]. Solid line: 4 K; dashed line: 300 K.

V_{GS} = [1.05 V; 2.17 V; 3.3 V]. Solid line: 4 K; dashed line: 300 K.

R.M. Incandela et al., *J. of EDS 2018*

I_D-V_{DS} Characterization (40nm)

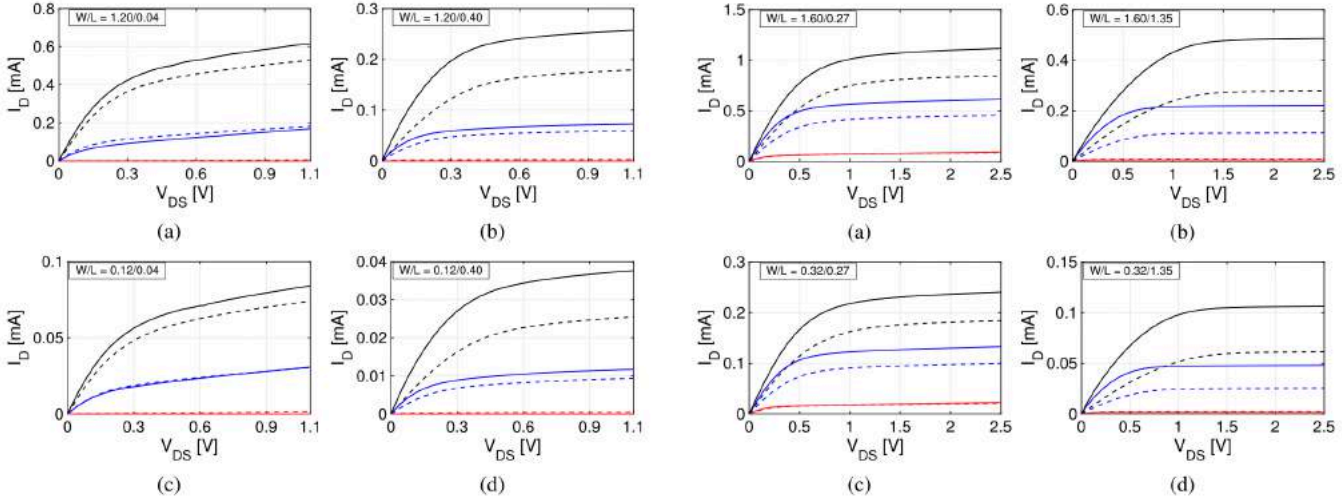

V_{GS} = [0.43 V; 0.76 V; 1.1 V]. Solid line: 4 K; dashed line: 300 K.

V_{GS} = [0.85 V; 1.68 V; 2.5 V]. Solid line: 4 K; dashed line: 300 K.

R.M. Incandela et al., *J. of EDS 2018*

I_D-V_{GS} Characterization

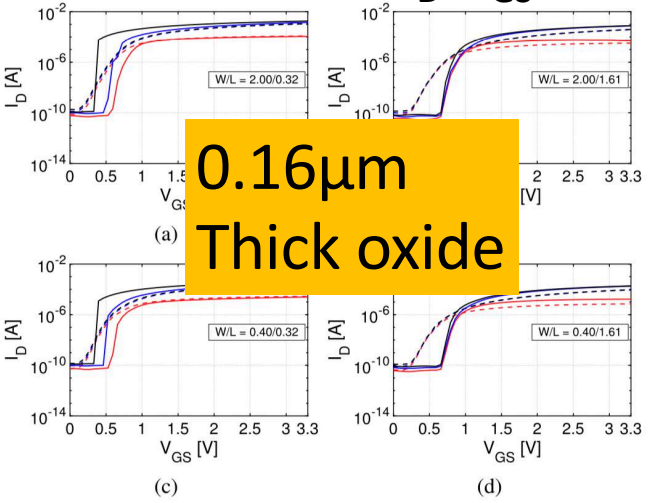

0.16µm
Thick oxide

V_{DS} = [0.1 V; 1.7 V; 3.3 V]. Solid line: 4 K; dashed line: 300 K.

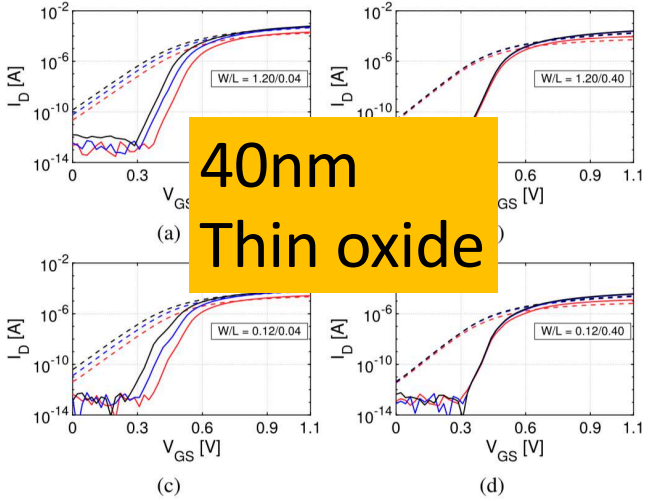

40nm
Thin oxide

V_{DS} = [0.1 V; 0.6 V; 1.1 V]. Solid line: 4 K; dashed line: 300 K.

R.M. Incandela et al., *J. of EDS 2018*

I_D-V_{GS} Characterization in Sub-K Regimes

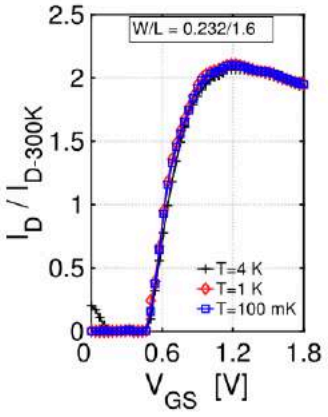

NMOS
VDS = 1.8V

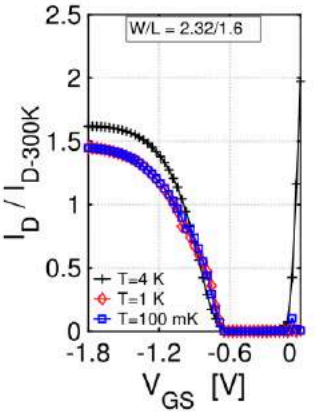

PMOS
VDS = -1.8V

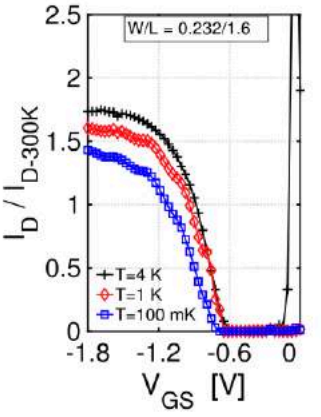

PMOS
VDS = -1.8V

R.M. Incandela et al., *J. of EDS 2018*

CMOS Modeling

MOS11 parameters for 0.16-μm CMOS					
BETSQR	VFBR	THESRR	SDIBLO	ALPR	KOR
THESATR	THERR	A1R	A2R	A3R	
PSP parameters for 40-nm CMOS					
FACTUO	DELVTO	THEMUO	THESATO	RSW1	CFL
ALPL	MUEO	FBET1			

Model

Measurement

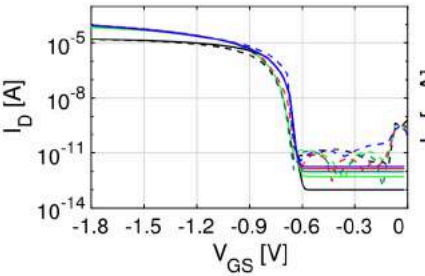

Thin oxide PMOS
V_{DS} = -1.8 – -0.09V

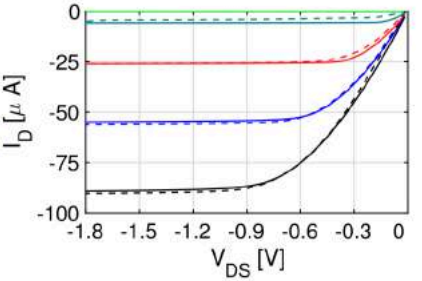

Thin oxide PMOS
V_{GS} = -1.3 – -1.8V

CMOS Modeling

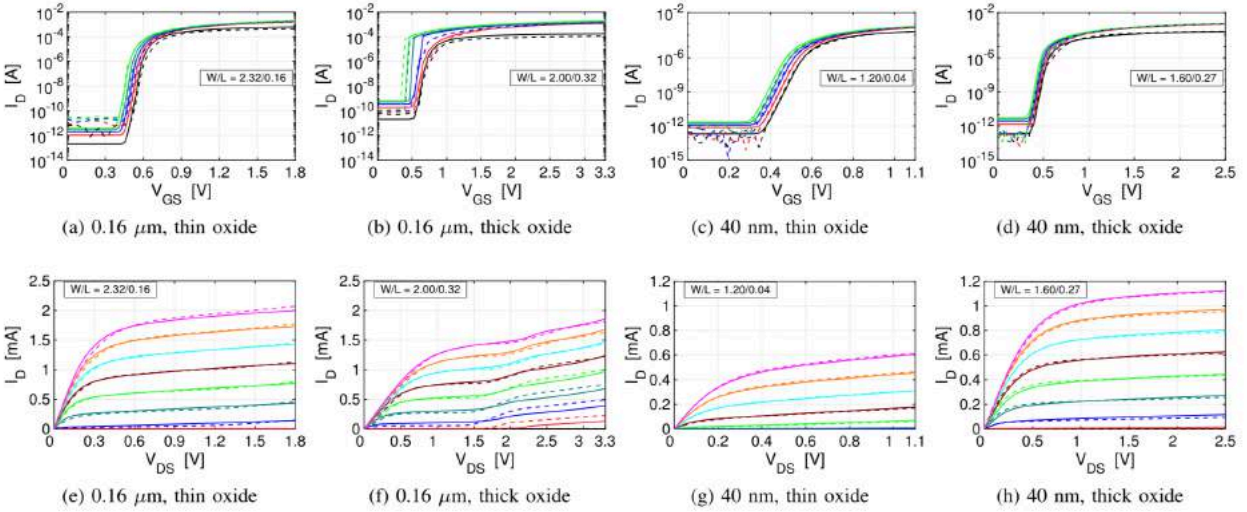

(a) 0.16 μm, thin oxide (b) 0.16 μm, thick oxide (c) 40 nm, thin oxide (d) 40 nm, thick oxide

(e) 0.16 μm, thin oxide (f) 0.16 μm, thick oxide (g) 40 nm, thin oxide (h) 40 nm, thick oxide

Sub-threshold Slope (SS)

$$SS = \ln(10)\frac{kT}{q}\left(1 + \frac{C_d}{C_{ox}}\right)$$

C_d = depletion layer capacitance
C_{ox} = gate oxide capacitance

$$SS = \ln(10)\frac{kT}{q} \sim 60\text{mV/dec}$$

$C_d = 0$; $C_{ox} \rightarrow$: thermionic limit

Sub-threshold Slope Characterization(SS)

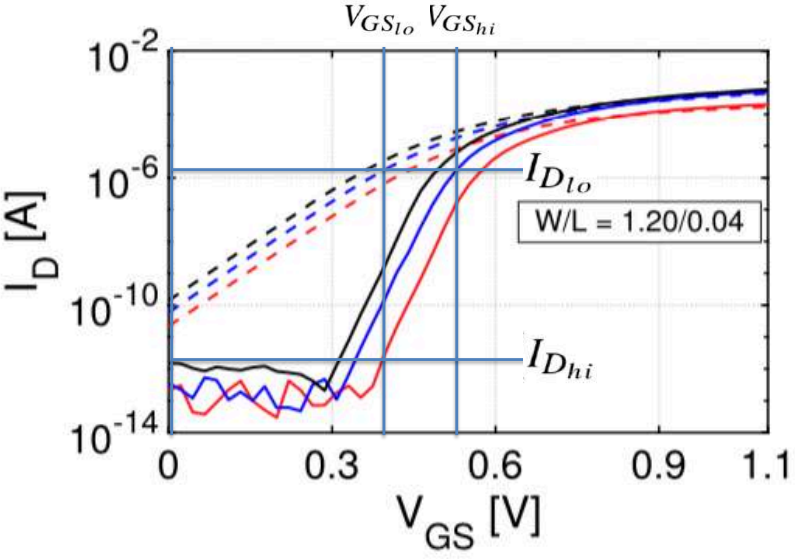

$$SS^{-1} = \frac{|\log\left(I_{D_{hi}}/I_{D_{lo}}\right)|}{V_{GS_{hi}} - V_{GS_{lo}}}$$

Sub-threshold Slope (SS)

PMOS W/L = 2.32µm / 1.6µm

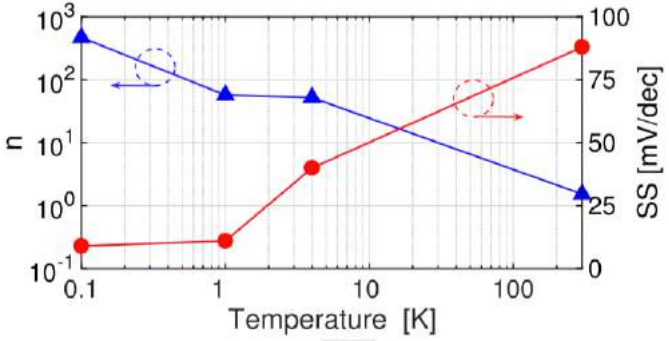

R.M. Incandela et al., *ESSDERC* 2017
R.M. Incandela et al., *J. of EDS 2018*

Substrate Resistivity

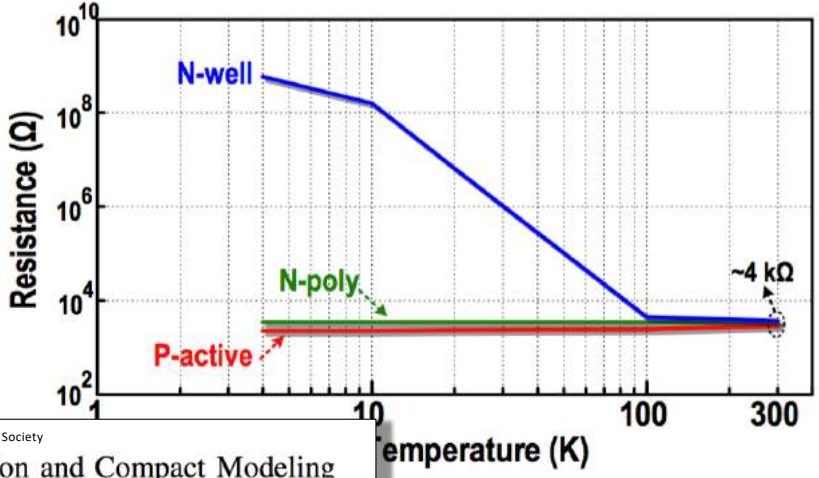

ra et al., *JSSC* 2018

IEEE Journal of the Electron Device Society

Characterization and Compact Modeling of Nanometer CMOS Transistors at Deep-Cryogenic Temperatures

Rosario M. Incandela, *Student, IEEE*, Lin Song, Harald Homulle, Edoardo Charbon, *Fellow, IEEE*, Andrei Vladimirescu, *Fellow, IEEE*, and Fabio Sebastiano, *Senior Member, IEEE*

Mismatch Modeling at Cryo

Subthreshold Current Mismatch: Why Do We Care?

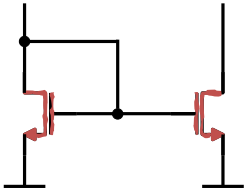

- Impacts performance of:
  - ADC/DAC
  - Differential pairs
  - SRAM

- Worsens with technology scaling

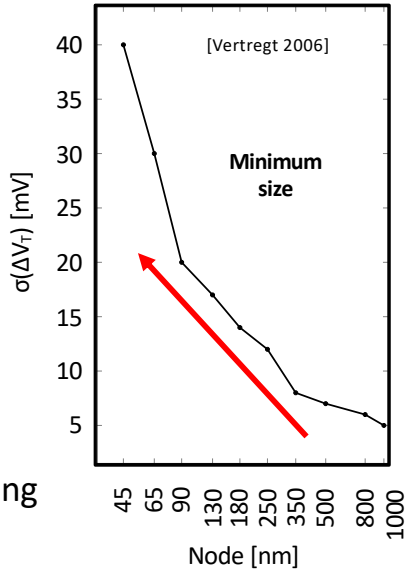

Subthreshold Current Model

$$I_D = I_0 e^{(V_{GS}-V_{TH})/SS}$$

Taylor expansion is impractical at cryo due to the instability of ID and the exponential nature of it.

Solve wrt $\log(I_D)$

$$\log(I_D) \propto \frac{1}{\ln(10)} \frac{V_{GS} - V_{TH}}{SS}.$$

Taylor expansion on V_{TH} and SS

$$\Delta \log(I_D) = \frac{1}{\ln(10)} \left(-\frac{1}{SS} \Delta V_{TH} - \frac{(V_{GS} - V_{TH})}{SS} \frac{\Delta SS}{SS} \right)$$

Subthreshold Current Model

$$\sigma^2_{\Delta \log I_D} = \frac{1}{\ln(10)^2}\left[\left(\frac{\sigma_{\Delta V_{TH}}}{\overline{SS}}\right)^2 + \left(\frac{V_{GS}-V_{TH}}{\overline{SS}}\frac{\sigma_{\Delta SS}}{\overline{SS}}\right)^2 + 2\frac{(V_{GS}-V_{TH})}{\overline{SS}^3}\sigma_{\Delta V_{TH}}\sigma_{\Delta SS}\rho_{\Delta V_{TH},\Delta SS}\right]. \quad (5)$$

The correlation factor ρ between V_{TH} and SS is generally negligible at 300K, 100K, and also at cryogenic temperatures.

Croon Model

$$\sigma^2_{\Delta I_D/I_D} = \ln(10)^2 \sigma^2_{\Delta \log I_D}$$

$$\sigma^2_{\Delta \log I_D} = \frac{1}{\ln(10)^2} \left[\sigma^2_{\Delta\beta/\beta} + \left(\frac{\bar{g}_m}{\bar{I}_D} \right)^2 \sigma^2_{\Delta V_{TH}} \right], \qquad (7)$$

Pelgrom Scaling Law

$$\sigma_{\Delta V_{TH}} = \frac{A_{VT}}{\sqrt{WL}} \qquad \sigma_{\Delta\beta/\beta} = \frac{A_{\beta}}{\sqrt{WL}} \qquad \sigma_{\Delta SS/SS} = \frac{A_{SS}}{\sqrt{WL}}$$

A_{VT} : area scaling parameter for V_{T}
A_{β} : area scaling parameter for β
A_{SS} : area scaling parameter for SS
W, L: transistor geometry parameters

How to Characterize Mismatch?

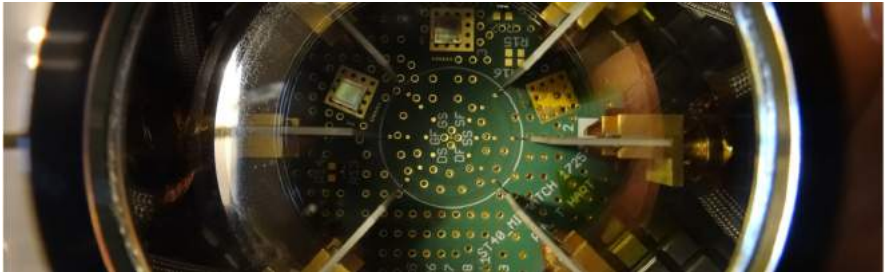

P. 't Hart et al., *ESSCIRC* 2018

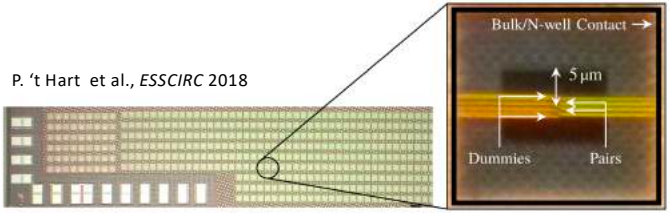

Fig. 1. Die micrograph (*left*) with close-up of a W/L = 1.2 µm/0.4 µm matched pair (*right*).

Mismatch Measurements

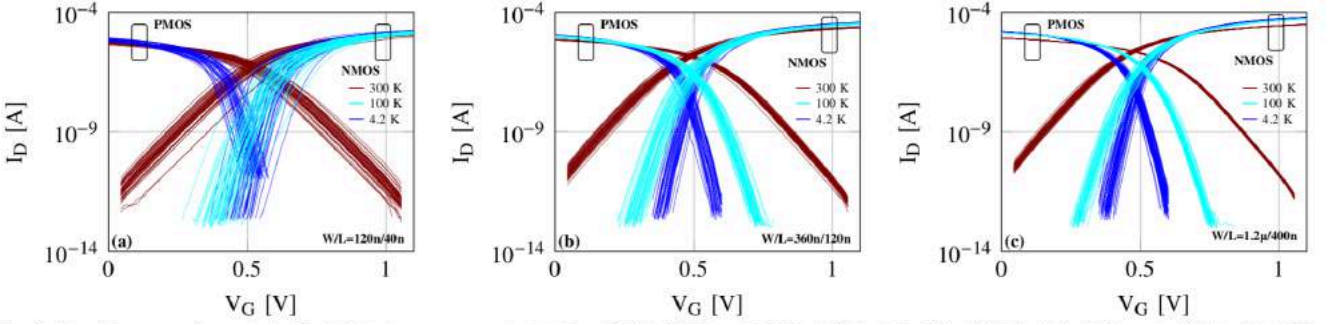

48 devices tested
$|V_{DS}|$ = 50mV, V_S=0V (NMOS)
$|V_{DS}|$ = 50mV, V_S=1.1V (PMOS)

P. 't Hart et al., *J. of EDS* 2020

Mismatch Measurements (2)

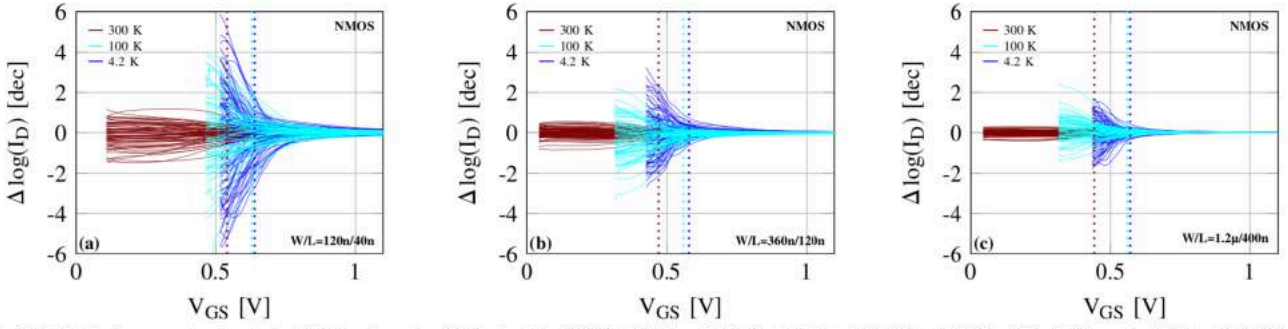

72 device pairs tested
V_{TH} in dashed lines
$|V_{DS}|$ = 50mV

P. 't Hart et al., *J. of EDS* 2020

Pelgrom Area Scaling Parameters

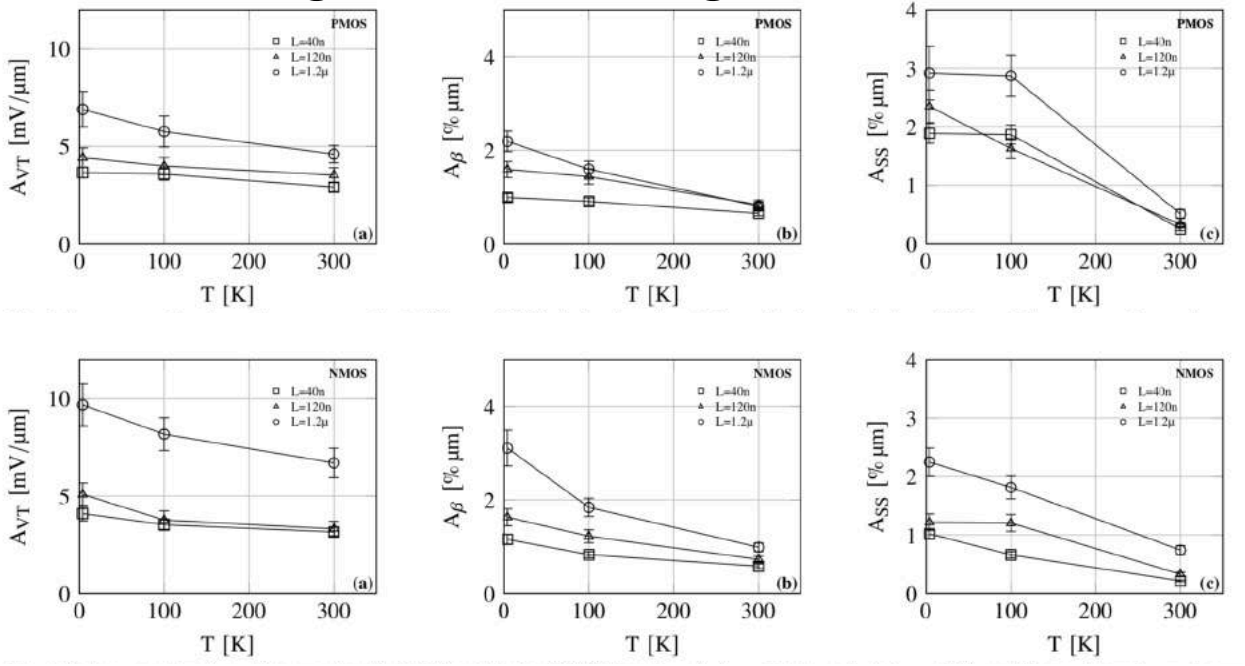

Mismatch Modeling

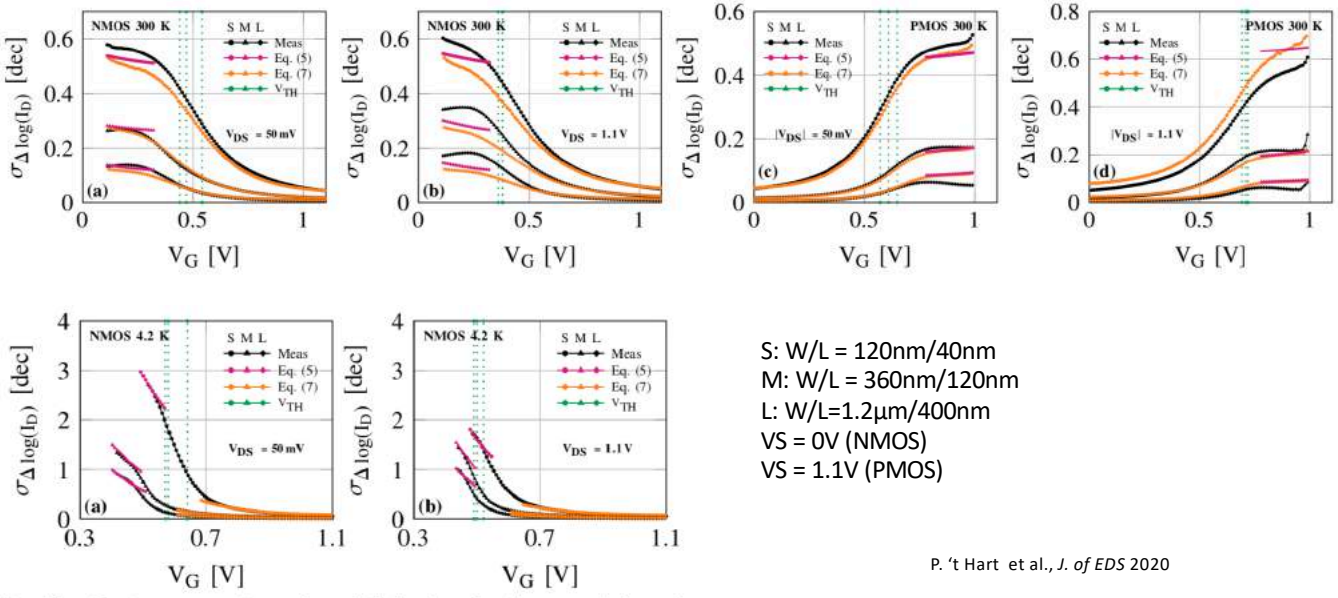

S: W/L = 120nm/40nm
M: W/L = 360nm/120nm
L: W/L=1.2µm/400nm
VS = 0V (NMOS)
VS = 1.1V (PMOS)

P. 't Hart et al., *J. of EDS* 2020

Position Dependence

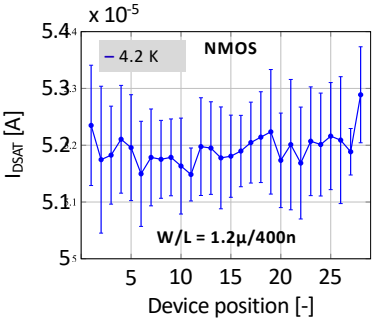

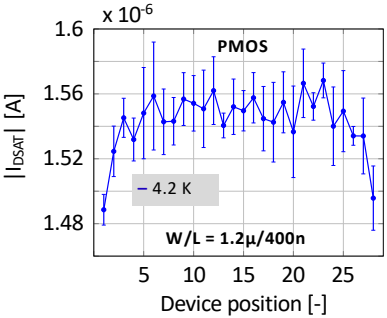

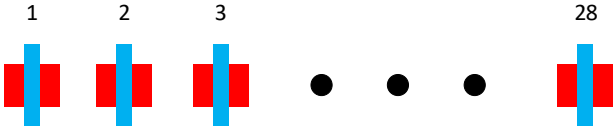

Summary on Threshold Mismatch

- Cryo-CMOS: mismatch follows Pelgrom and Croon models
- Fixed V_{GS} biasing ➞ matching deteriorates up to 10x
- Fixed G_m/I_D biasing ➞ matching deteriorates “only” 1.1x

Digital Modeling at Cryo

Lowerbound in Digital Design

$$V_{DD,min} \approx 2\frac{kT}{q}\ln(2) = 36\text{mV}$$

CMOS circuits operate in subthreshold wherever this equation holds

$$I_{DS} = I_0 \frac{W}{L} e^{\frac{V_{GS}-V_{TH}}{nv_t}} \left(1 - e^{-\frac{V_{DS}}{v_t}}\right);\ I_0 = \mu_0 C_{ox} \frac{W}{L} (n-1) v_t^2,$$

n is the sub-threshold slope (SS) factor and $v_t = kT/q$,

The net effect in sub-threshold regimes is a decrease of leakage currents by orders of magnitude, implying a significant increase in the I_{ON}/I_{OFF} ratio

Lowerbound in Digital Design

Assuming an ideal SS factor $n = 1$, at 4.2 K, according to well established room temperature models, one could theoretically achieve $V_{DD,min} \approx 2\ln(2)v_t = 0.48\text{mV}$.

However, at 4.2 K the consensus is that $n \approx 34.9$. Thus, this fundamental limit is actually $V_{DD,min} \approx 2.47\text{mV}$. Additional non-idealities include reverse short-channel effect (RSCE) and inverse narrow-width effect (INWE).

Both effects substantially modulate the threshold voltage.

Latchup

Latch-up has been found to be unpredictable in deep-cryogenic operation. Latch-up immunity typically improves at temperatures lower than RT, thanks to lower well and substrate resistance and to higher base-emitter voltages and lower current gain of parasitic bipolar transistors. However, shallow level impact ionization (SLII), a mechanism for carrier generation, emerges below 50 K

Recommendations

A) create extensive substrate contacts and well-taps, so as to minimize the chance of latch-up at 4.2 K;
B) resize the transistors, so as to reduce INWE and thus maximize V_{TH} modulation;
C) add secondary power rails to enable forward back-biasing, so as to compensate for an increase of V_{TH} at 4.2, in addition use low-V_{TH} transistors;
D) minimize the length of transistors (in contrast to conventional RT sub-threshold standard cell design, where the opposite is generally done);
E) when useful, make the layout aware of mismatch by increasing the overall height of the cells.

Summary of Issues 300K –> 0.1K

- Threshold voltage increases significantly
- A current kink may appear
- Mismatch in passives and actives is more prominent
- The substrate becomes practically floating
- The SS is higher but it saturates around 1K
- Leakage drastically reduces

Trends and Predictions

- How will devices perform in 5 years at 77K?
- How will FinFETs/nanowire FET behave at 77K (Lg<20nm)
- Will ballistic transport affect these devices?
- How different will optimization be at 77K?
- Is there a way to decrease V_T?

High-Level Modeling at Cryo

High-Level Modeling: SPINE (SPIN Emulator)

Objectives:

- Enable co-design qubit/electronics
- Derive specifications for Horse Ridge and other components
- Minimize power to achieve wanted fidelity

Circuit simulator

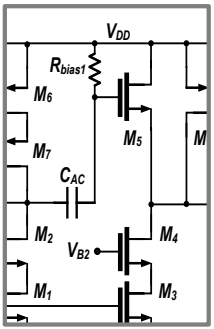

Electrical signals

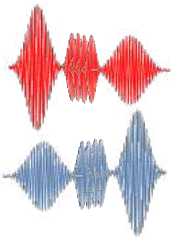

Fidelity (read-out)

Qubit simulator (Hamiltonian)

Fidelity

SPINE

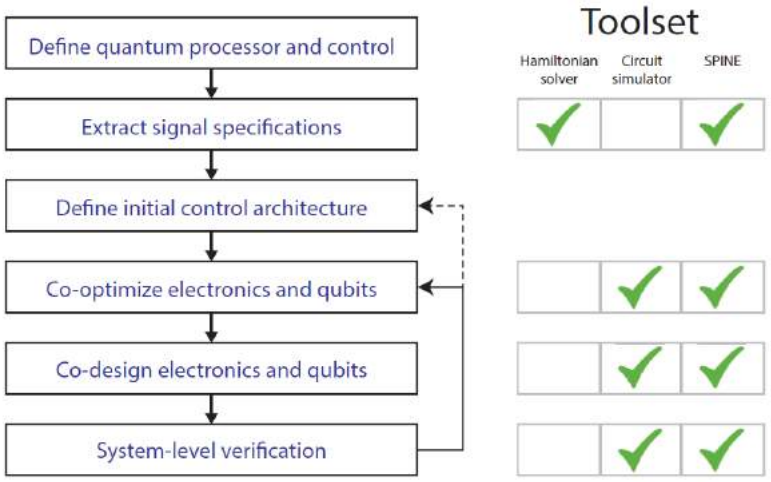

J. Van Dijk *et al.*, DATE 2018

SPINE

- Microwave Carrier: **Keysight E8267D**
  - 22.4 kHz resolution — 1 mHz
  - $\mathcal{L}$ (1 MHz) = -106 dBc/Hz — >15 dB better
  - S_n = 7.12 nV/√Hz — 63 nV/√Hz
    → > 20 dB attenuation

- Microwave Envelope: **Tektronix 5014C**
  - 8-bit resolution — 14-bit
  - 140 MS/s — 1.2 GS/s
  - 3.56 ns_{rms} — 5.0 ps_{rms}
  - 40 dB SNR — better

With SPINE we checked that these specs are enough

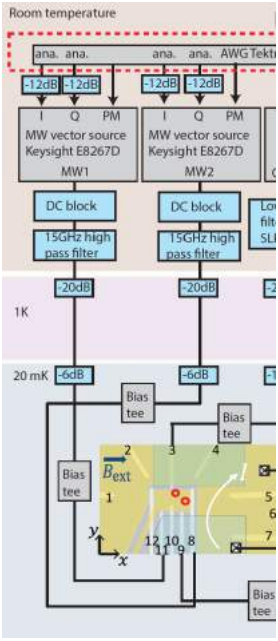

SPINE

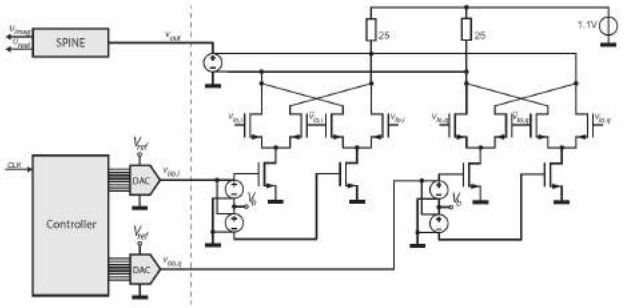

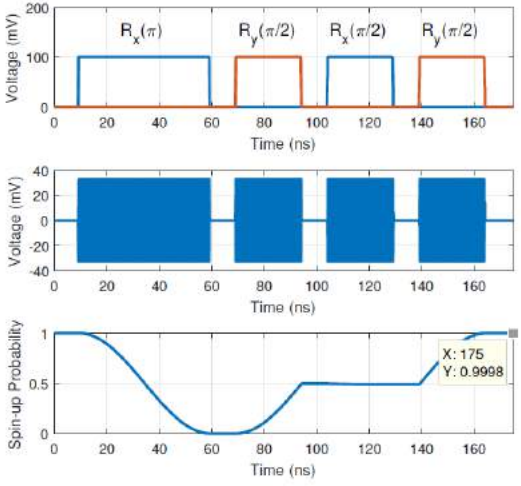

- Example of full simulation:
  - Sequence of rotations
  - Resulting RF signals
  - Qubit response, in terms of spin-up probability
- This involves spin emulation, M/S simulation, RF simulation

J. Van Dijk *et al.*, DATE 2018

Cryogenic Reconfigurable Hardware

Cryo-FPGAs

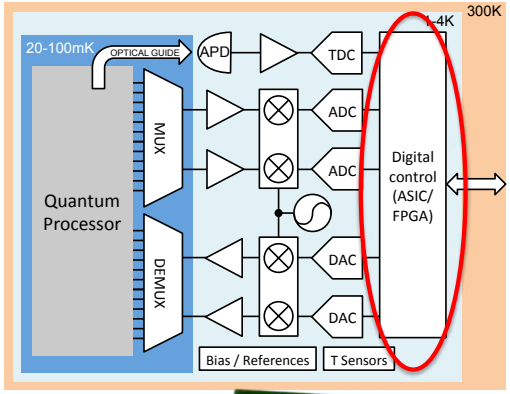

Cryo-FPGAs

CryoCMOS Hardware Technology
A Classical Infrastructure for a Scalable Quantum Computer

ACM Frontiers in Computing, Como 2016

Harald Homulle[1], Stefan Visser[1], Bishnu Patra[1], Giorgio Ferrari[2], Enrico Prati[3], Carmen G. Almudéver[1], Koen Bertels[1], Fabio Sebastiano[1], Edoardo Charbon[1]

[1]QuTech, Delft University of Technology, Delft, The Netherlands

[2]Politecnico di Milano, Milano, Italy, [3]Consiglio Nazionale delle Ricerche, Milano, Italy

{h.a.r.homulle, f.sebastiano, e.charbon}@tudelft.nl

FPGA functionality

- All FPGA components are working in the cryogenic environment down to 4K
- No modifications required

Component	Functional	Behavior
IOs	✓	
LVDS	✓	
LUTs	✓	Delay change < 5%
CARRY4	✓	Delay change < 2%
BRAM	✓	No corruption (800 kB)
MMCM	✓	Jitter reduction of roughly 20%
PLL	✓	Jitter reduction of roughly 20%
IDELAYE2	✓	Delay change of up to 30%
DSP48E1	✓	No corruption over 400 operations

FPGA Performance

Specs:
Carry: 20 vs. 8.4 ps at 300 K
LUTs: 238 vs 235 ps at 300 K
Speed-up 2.4 vs 10.8% toward 300 K

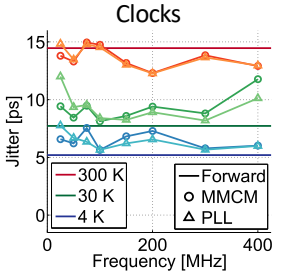

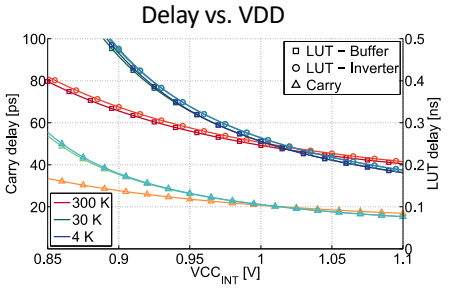

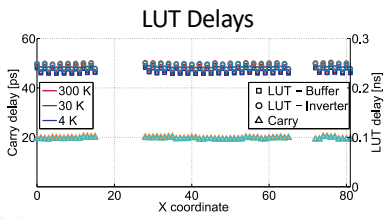

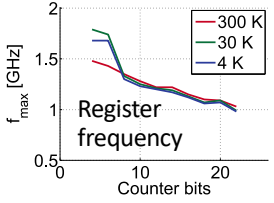

ADC on FPGA (1.2GSa/s)

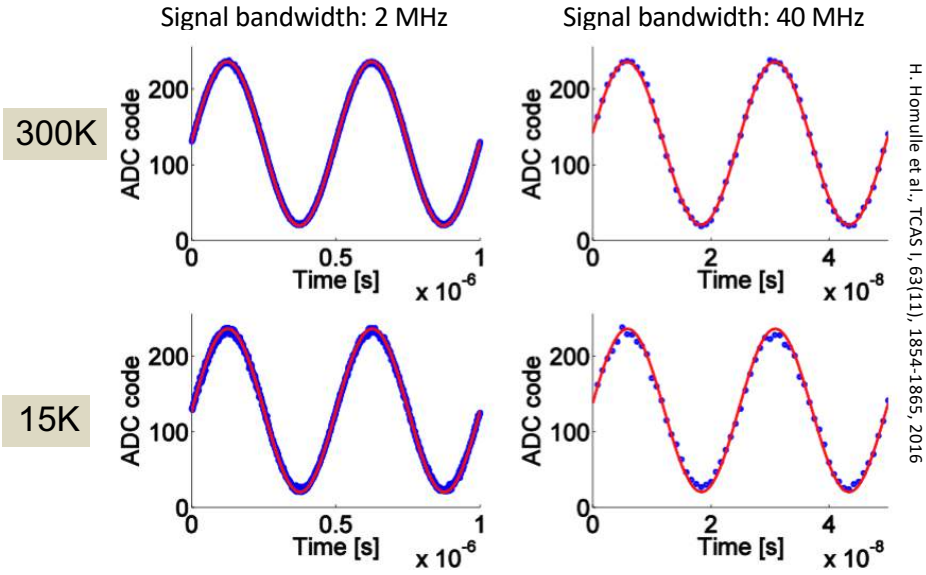

H. Homulle et al., TCAS I, 63(11), 1854-1865, 2016

ADC on FPGA

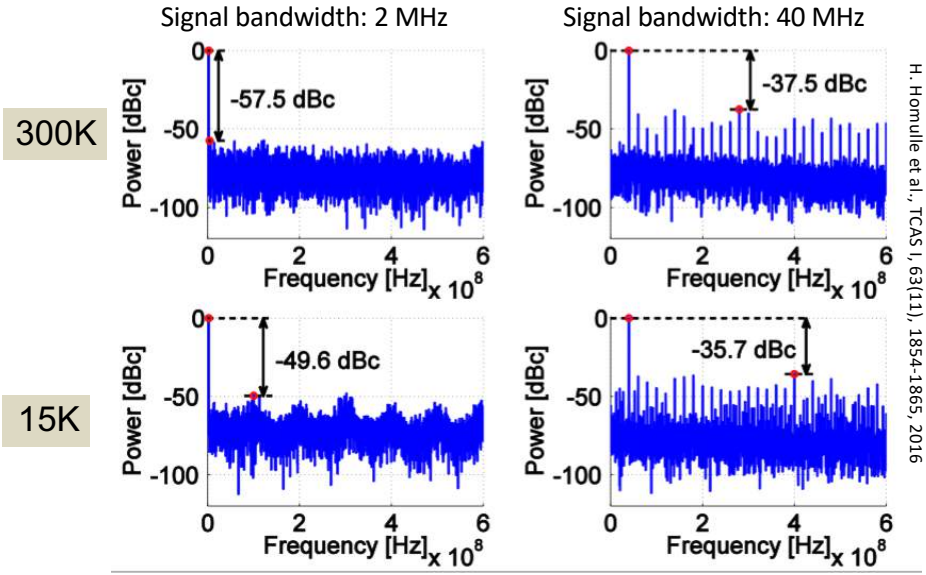

H. Homulle et al., TCAS I, 63(11), 1854-1865, 2016

Distortion (IM2, IM3)

- Two tones: ≈ 36 / 41 MHz
  - IM2 = 38 dB
  - IM3 = 46 dB
- Many secondary harmonics
- Interference with 100 MHz (sampling tone)

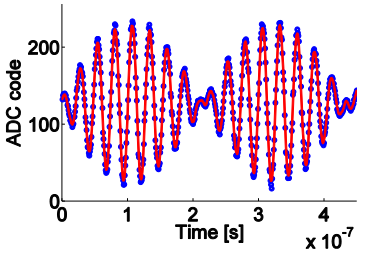

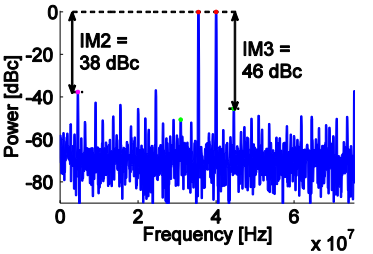

H. Hornulle et al., TCAS I, 63(11), 1854-1865, 2016

Cryogenic ASICs

Low Noise Amplifiers (Cryo-LNAs)

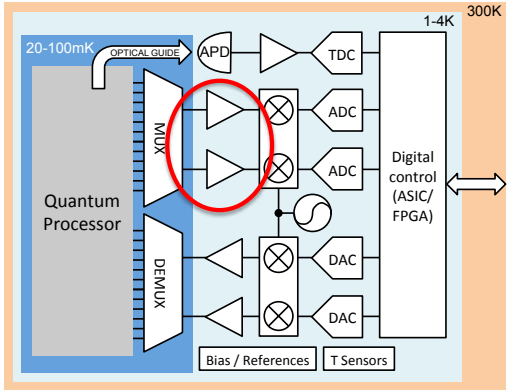

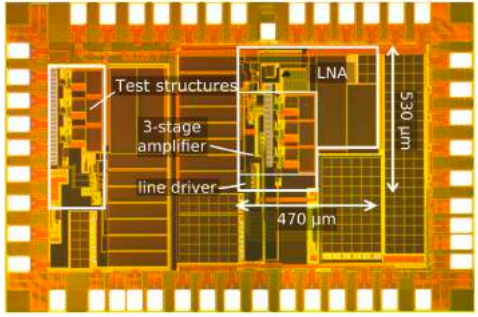

Cryo-LNA

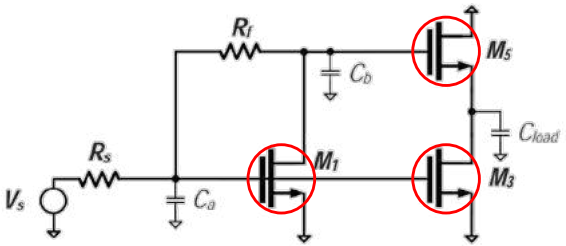

F. Bruccoleri et al., *JSSC* 2004

- Standard 160nm CMOS
- 500 MHz Bandwidth
- 0.1dB Noise figure
- 7K noise-equivalent temperature

Cryo-LNA

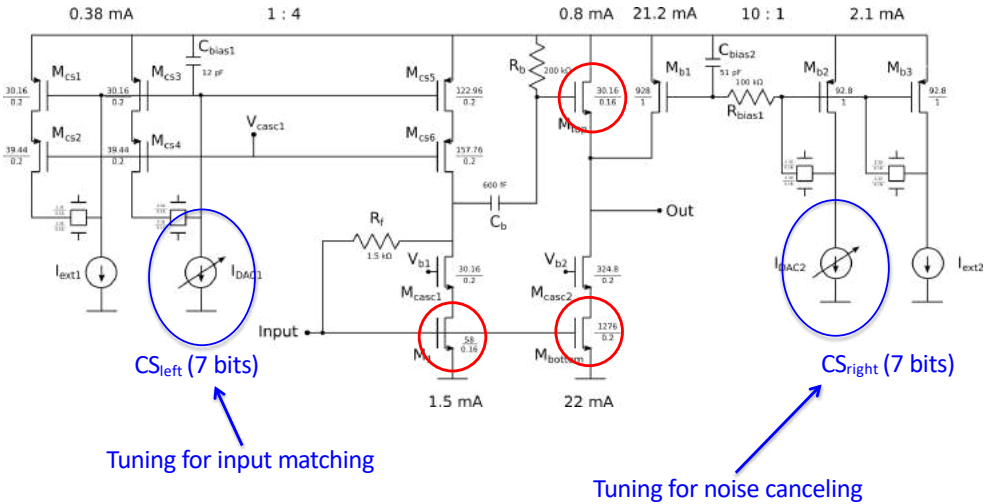

Noise Figure at RT

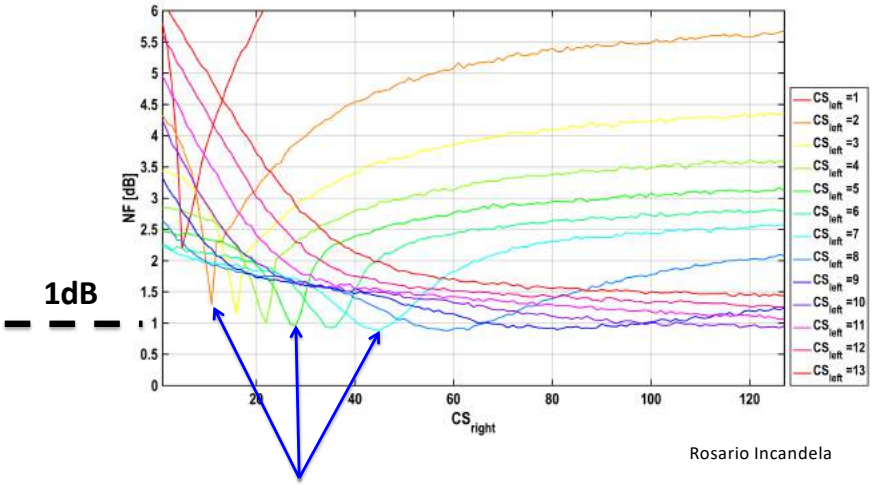

Rosario Incandela

Noise Figure at 4K

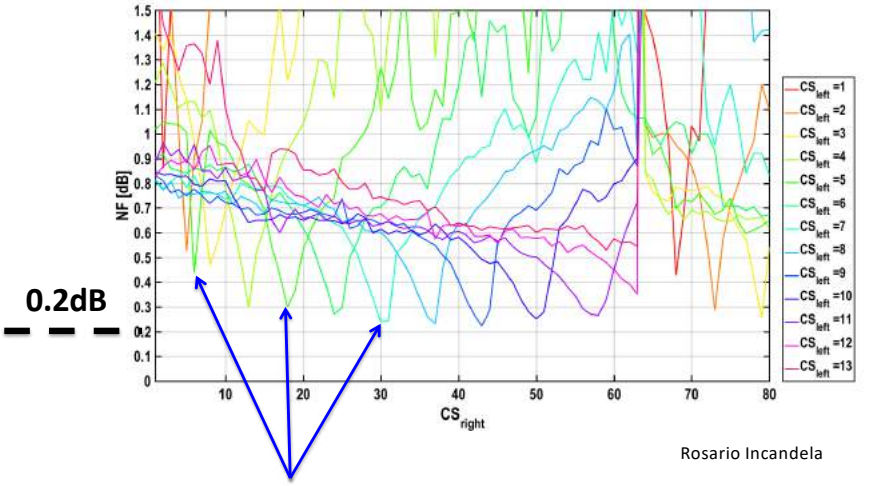

Gain and Noise

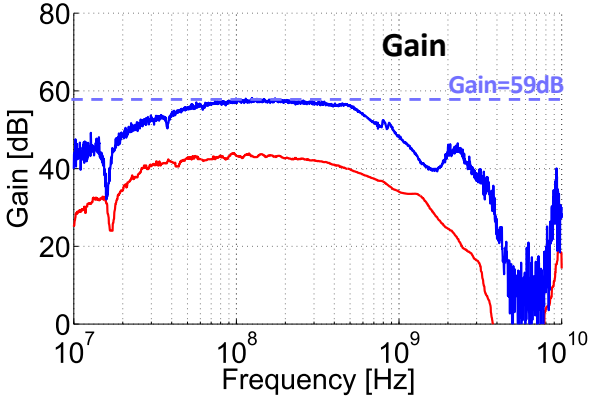

B. Patra, R. Incandela et al, *JSSC* 2018

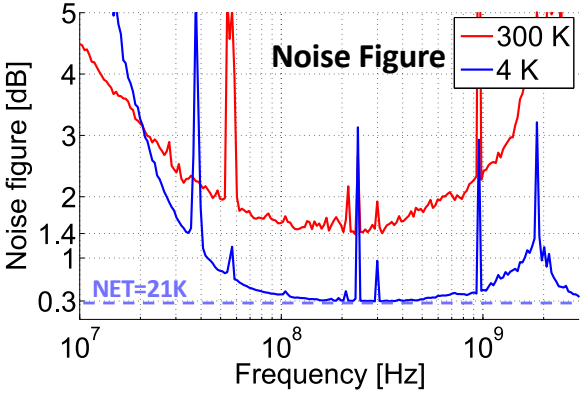

Power

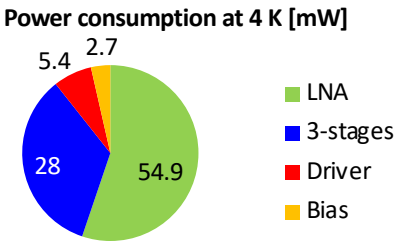

Measured: **91mW**

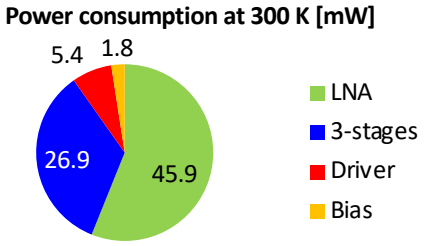

Measured: **80mW**

Sharing 150x 1MHz-channels (one channel per qubit)

=

0.61mW per qubit

Rosario Incandela

Can We Do Better?

Amplifier Metrics	Cryogenic HEMT 	JPA 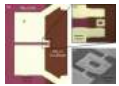	TWPA 1.0 	TWPA 2.0 
Power Dissipation	16 mW	100 pW	1 nW	5 nW
Bandwidth (>15 dB gain)	11 GHz	100 - 200 MHz	6 GHz	5 GHz
1-dB Compression point	0 dBm	-110 dBm (3 qubits)	-95 dBm (20-30 qubits)	-85 dBm (> 100 qubits)
Noise Temperature	5 K	400 mK	400 mK	400 mK
External Hardware	Isolator	Direct. Coupler, Circulator	Direct. Coupler	None

Courtesy: David Hover and Greg Calusine, MIT Lincoln Laboratory

Can We Do Better?

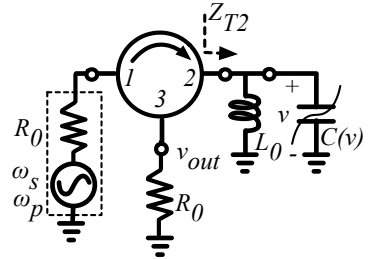

$$y_{NL}(j\omega_s) \approx -\omega_s \omega_i (\alpha_p C_0)^2 Z^*_{2,C_0}(j\omega_i)$$

$$\alpha_p \equiv K_1 V_p$$

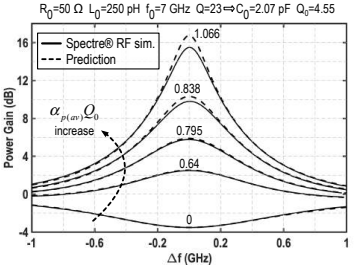

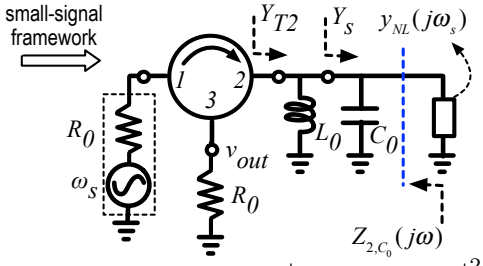

$$G_{T_{\max}}\big|_{Q\to\infty} = \left|\frac{1+(\alpha_p Q_0)^2}{1-(\alpha_p Q_0)^2}\right|^2$$

Major challenges:

- Narrowband
- Phase sensitive
- Large pump signal
- T_n limit of 4K @ 4K

CMOS Parametric Amplifier

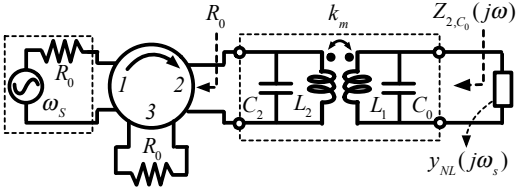

1) Transformer-based parametric amplifier

- ✓ Allow for broadband operation

2) CM impedance peaking

- ✓ Suppress the pump signal leak
- ✓ Reduce pump power consumption

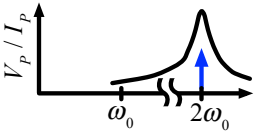

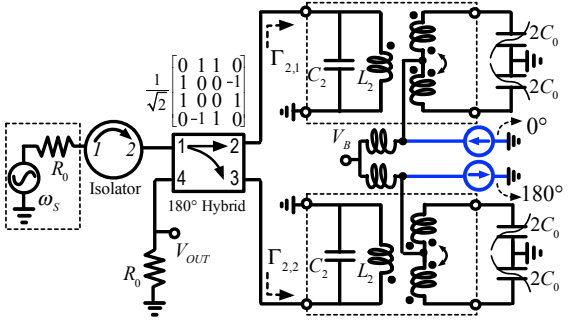

3) "image"–rejection architecture

- ✓ Double the usable RF bandwidth
- ✓ Phase-insensitive operation
- ✓ Allow for T_n limit of below 4K

M. Mehrpoo, F. Sebastiano, E. Charbon, M. Babaie, *Solid-State Circuit Letters*, 2020

CMOS PA Architecture

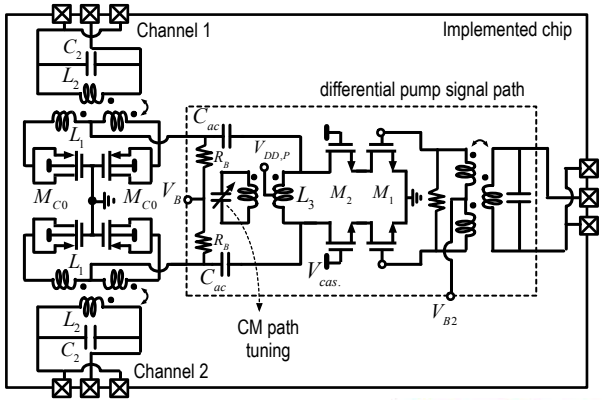

M. Mehrpoo, F. Sebastiano, E. Charbon, M. Babaie, *Solid-State Circuit Letters*, 2020

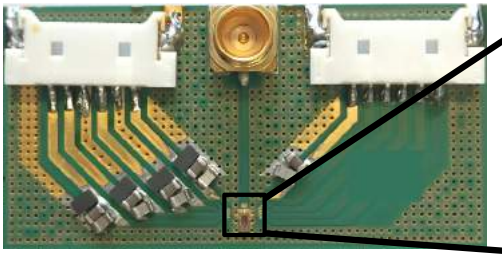

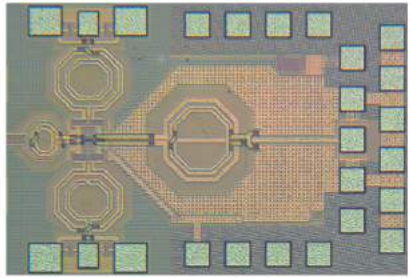

0.825 mm^2

Spectrum of Single Tone

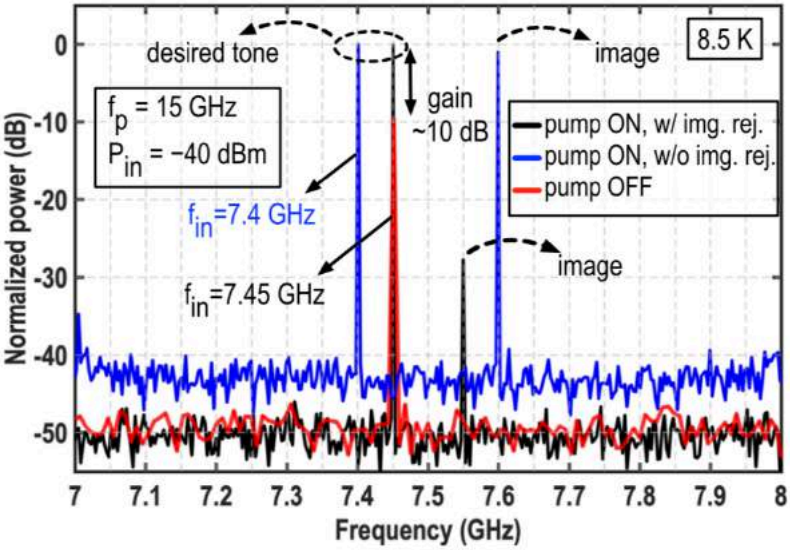

M. Mehrpoo, F. Sebastiano, E. Charbon, M. Babaie, *Solid-State Circuit Letters*, 2020

Power Gain vs. Pump Frequency and Temperature

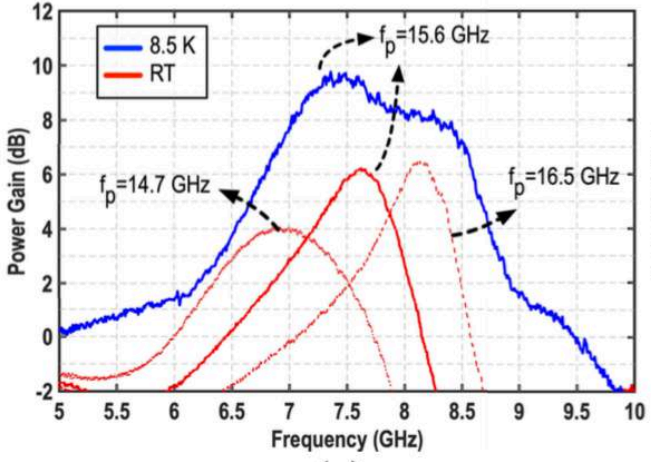

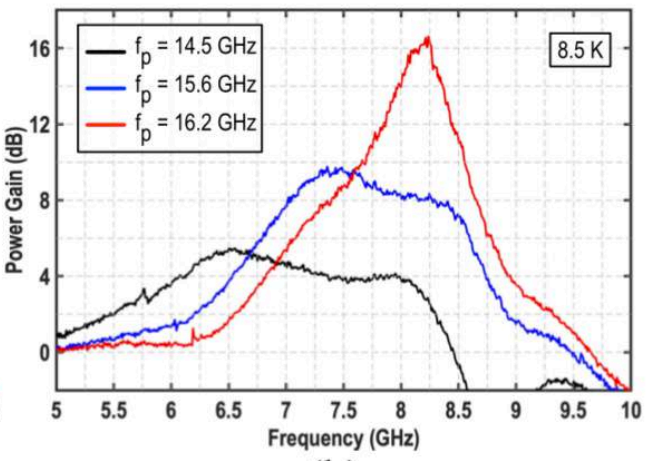

M. Mehrpoo, F. Sebastiano, E. Charbon, M. Babaie, *Solid-State Circuit Letters*, 2020

Image Rejection

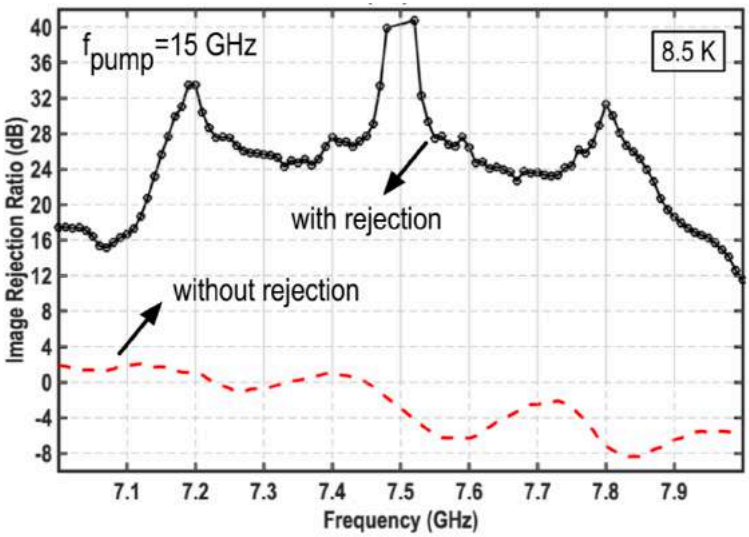

M. Mehrpoo, F. Sebastiano, E. Charbon, M. Babaie, *Solid-State Circuit Letters*, 2020

***CMOS Passive Circulators & Multiplexers

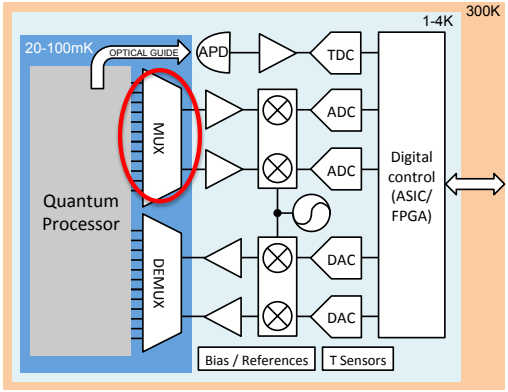

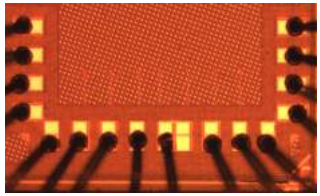

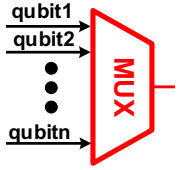

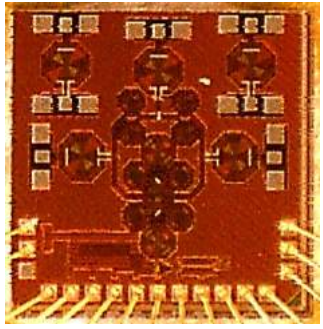

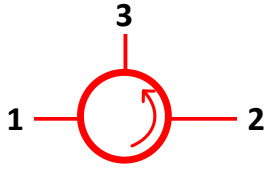

Transmission Line Circulator

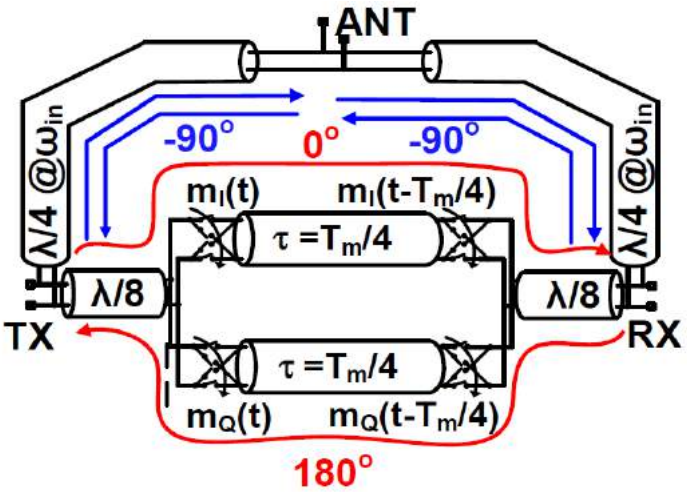

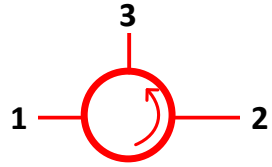

S-parameters at $\omega_{in} = 3\omega_m$

$$S = \begin{bmatrix} 0 & 0 & -1 \\ -j & 0 & 0 \\ 0 & -j & 0 \end{bmatrix}$$

Passive Circulator Architecture

- Non-reciprocal behavior due to staggered commutation
- Passive LC all-pass filters
- Passive mixers with non-overlapping I/Q phases
- On-chip LO divider and I/Q generation
- SPI control for tunability

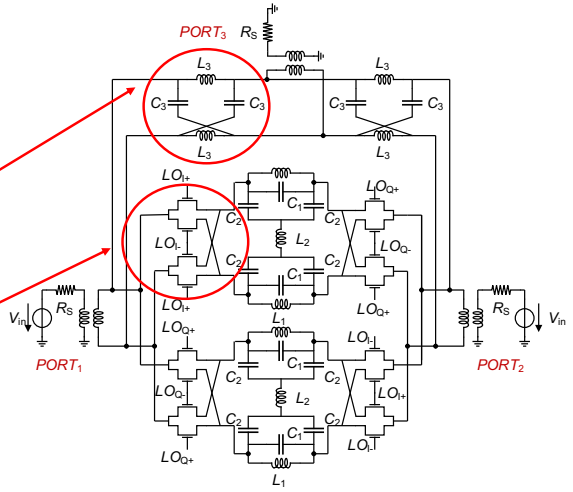

P_{DC} = 1.7 mW
P_{AUX} = 8 mW

Passive Circulator Architecture

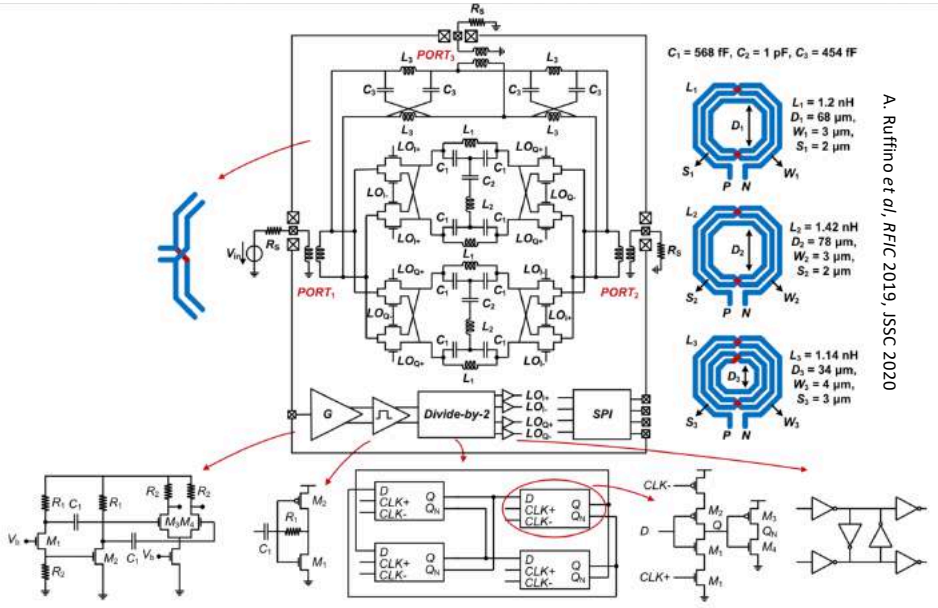

A. Ruffino *et al*, *RFIC* 2019, JSSC 2020

CMOS 40 nm Circulator Prototype

- TSMC CMOS 40 nm technology
- Tape-out, PCB design and measurements at 300 K and 4.2 K
- RF probing with LakeShore CPX probe station

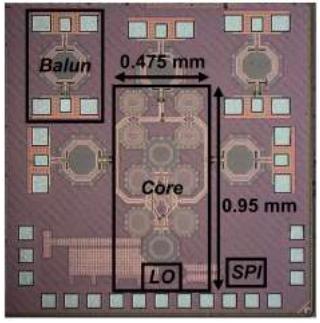

A. Ruffino *et al*, *RFIC* 2019, JSSC 2020

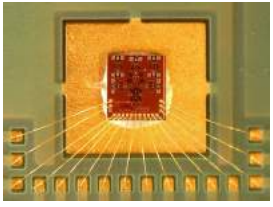

Measured S-parameters (300K)

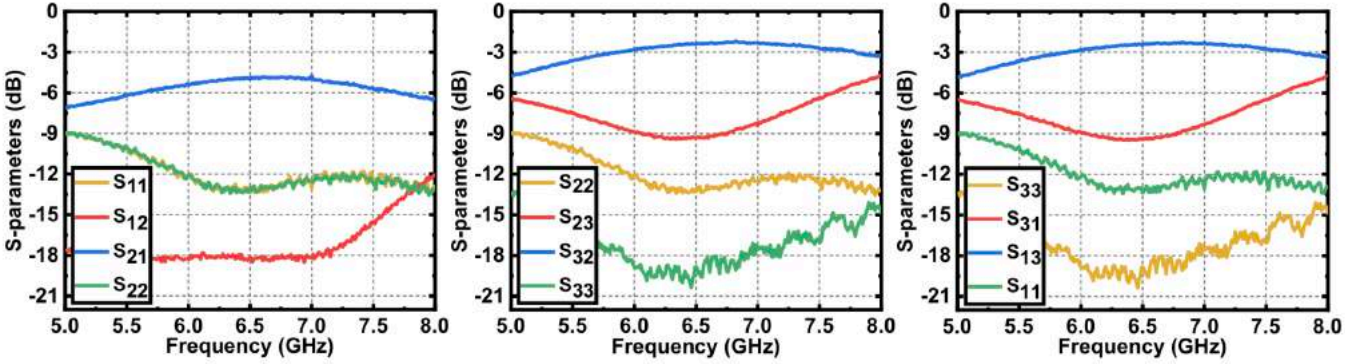

A. Ruffino *et al*, *RFIC* 2019, JSSC 2020

Measured S-parameters (4.2K)

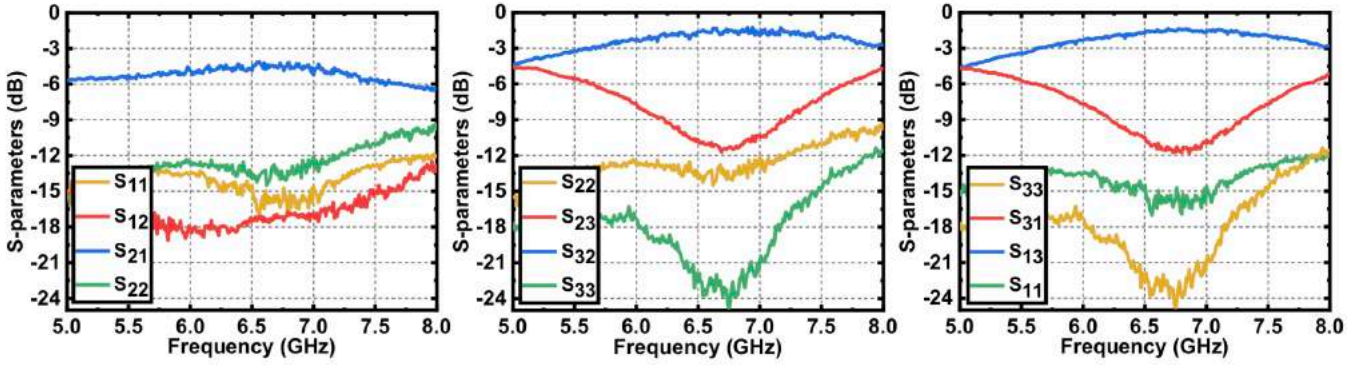

A. Ruffino *et al*, *RFIC* 2019, JSSC 2020

Circulator Noise Figure (300K)

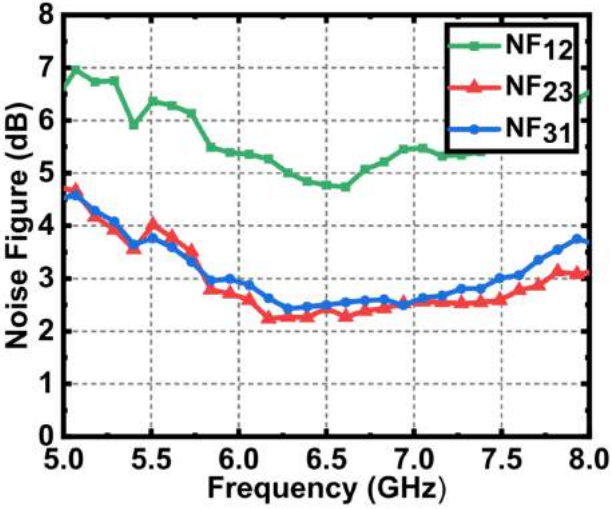

Minimum noise figure of 2.1 dB is measured, consistent with insertion loss measurements. There is no excess noise from clock generation path.

Circulator Linearity (300K)

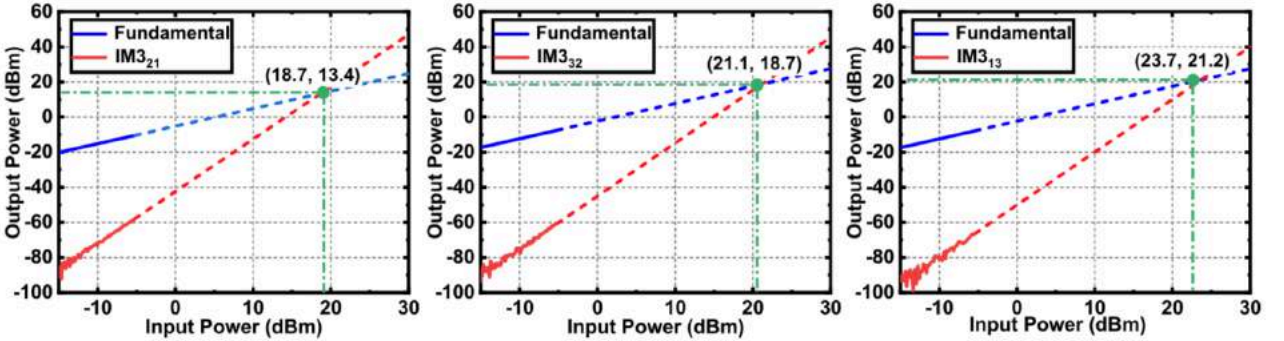

A. Ruffino *et al*, *RFIC* 2019, JSSC 2020

High linearity is measured in all directions, due to the quasi-passive nature of the circulator.

Circulator Linearity (4.2K)

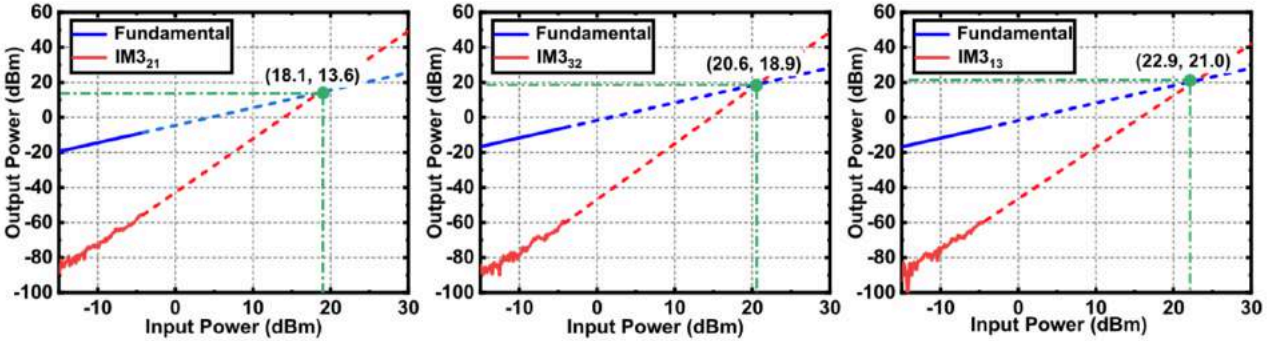

A. Ruffino *et al*, *RFIC* 2019, JSSC 2020

High linearity is measured in all directions, due to the quasi-passive nature of the circulator.

Circulator Summary

	This work	[5]	[4]	[6]	[7]
Technology	40-nm CMOS	65-nm CMOS	45-nm SOI	180-nm SOI	Ferrite
Working temperature (K)	4.2-300	300	300	300	0.02-300
Architecture	All-pass	N-path	T-line	T-line	Discrete
Frequency (GHz)	5.6-7.4	0.61-0.97[1]	22.7-27.3	0.86-1.08	4-8
Modulation index	5	1	3	3	N.A.
Insertion loss (dB)	2.2	1.7	3.2	2.1	0.4
Isolation (dB)	18	>20	18.5	>25	18
Fractional bandwidth[2] (%)	28	4.3	18	17	66
Noise figure (dB)	2.4-3.4	4.3	3.3-4.4	2.9-3.1	0.4
IIP3 (dBm)	>+17.5	+27.5	+20.1	+50	N.R.
Core area (mm^2)	0.45	25	2.16	16.5	1575
Power consumption (mW)	2.5/12.4[3]	59	78.4	170	0
Normalized power P_{DC}/f_0 (mW/GHz)	1.9	75	3.1	175	0

[1]Range of center frequency tunability, [2]Isolation and 1-dB insertion loss bandwidth, [3]Core (divider and mixer buffers) power and overall power consumption respectively.

Cryo-Oscillators

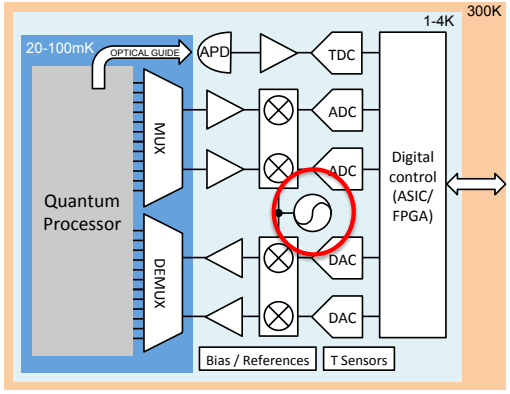

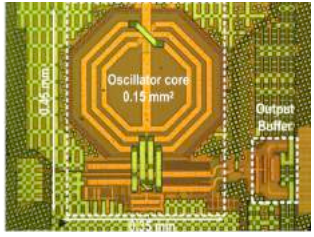

Cryo-Oscillator (Class F)

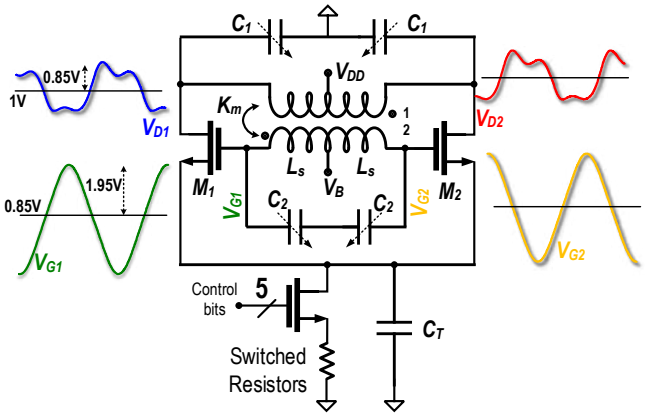

M. Shahmohammadi, *ISSCC* 2015

Phase Noise

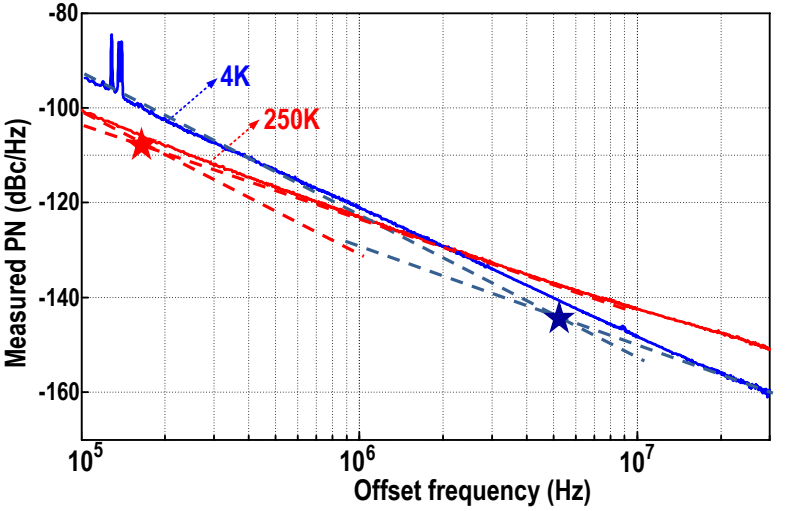

Measured Phase Noise

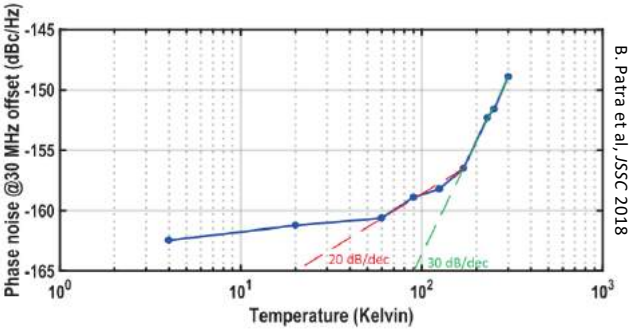

B. Patra et al, JSSC 2018

Curtesy: Masoud Babaie

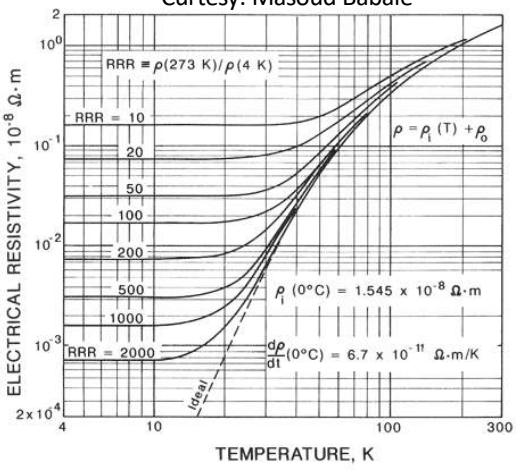

Source: copper.org

Sources of noise:

- Thermal noise
- Shot noise
- Impurities in copper

Frequency Stability

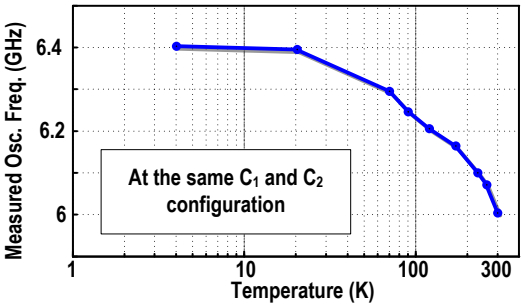

B. Patra et al, *JSSC* 2018

Improving Frequency Stability

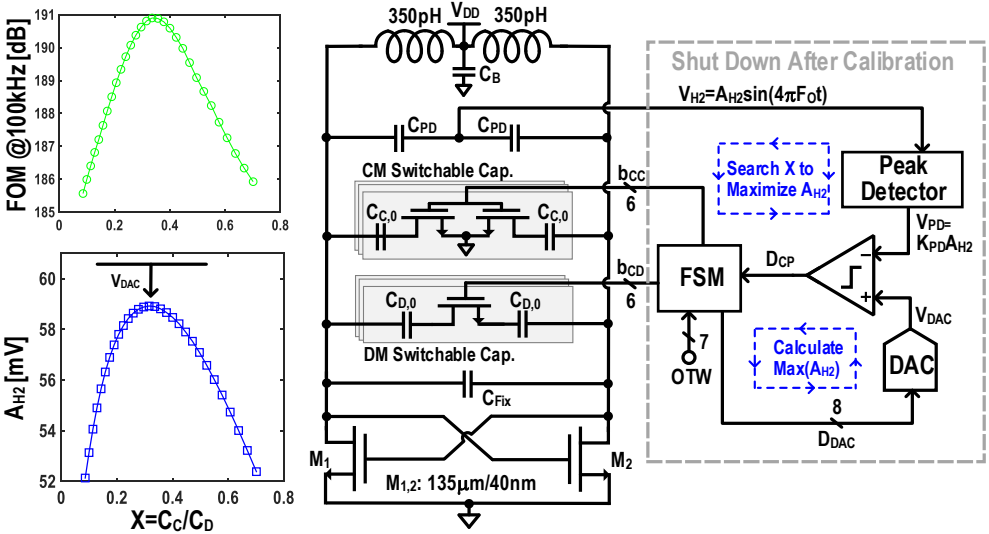

Improving Frequency Stability (2)

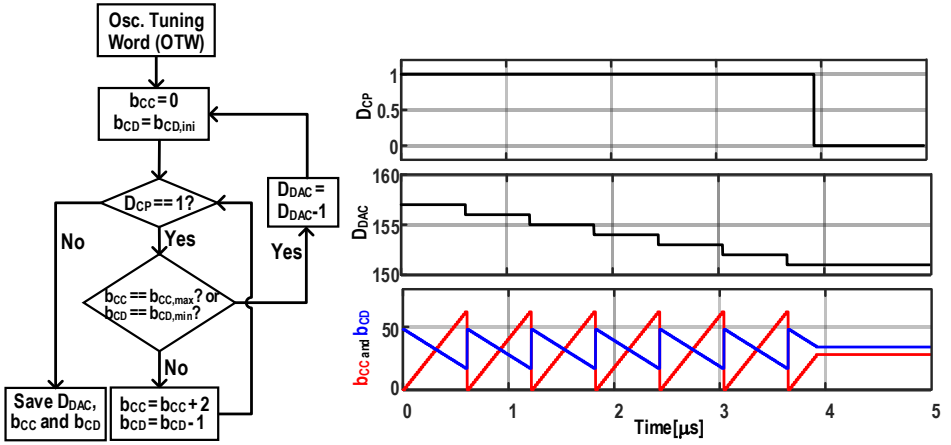

J. Gong, F. Sebastiano, E. Charbon, M. Babaie, *ISSCC* 2020

Phase Noise at 300K

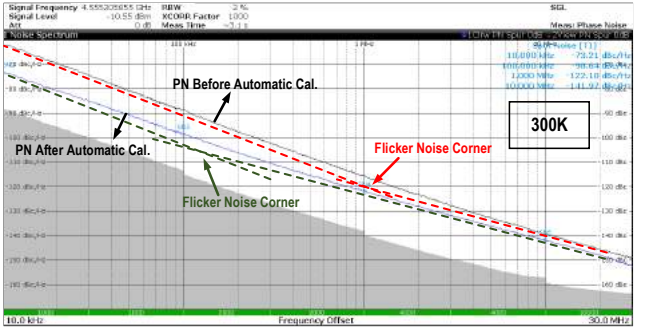

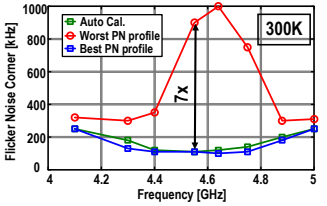

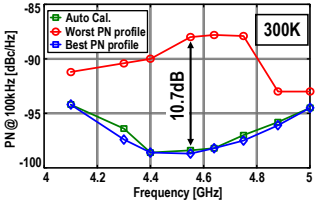

J. Gong, F. Sebastiano, E. Charbon, M. Babaie, *ISSCC* 2020

Phase Noise at 4K

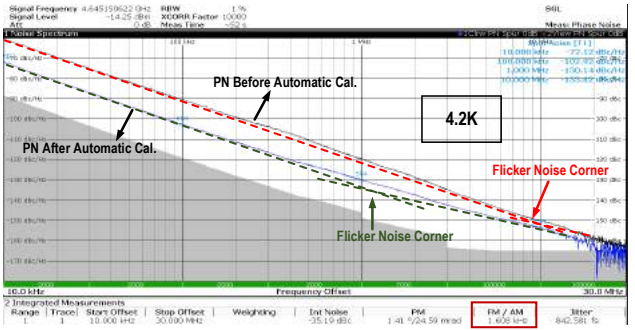

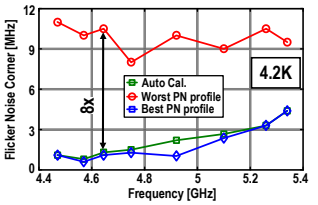

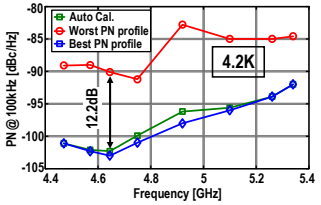

J. Gong, F. Sebastiano, E. Charbon, M. Babaie, *ISSCC* 2020

Implementation in 40nm CMOS Node

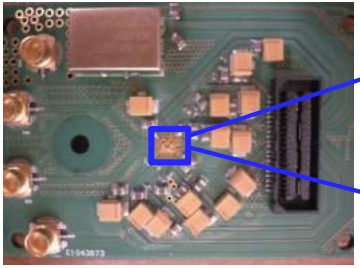

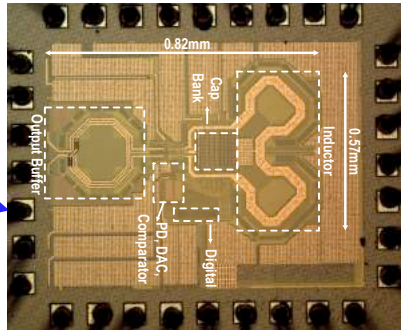

Measurements at RT:
Technology: 40nm CMOS
F_{out}: 4.05-5.16GHz (24.1%)
F_{ref}: 20MHz
Supply: 0.5V (oscillator core)
Power consumption: 3.2mW
PN @10MHz: -141.5dBc/Hz
PN@100kHz:-98.8dBc/Hz

Cryo-Logic

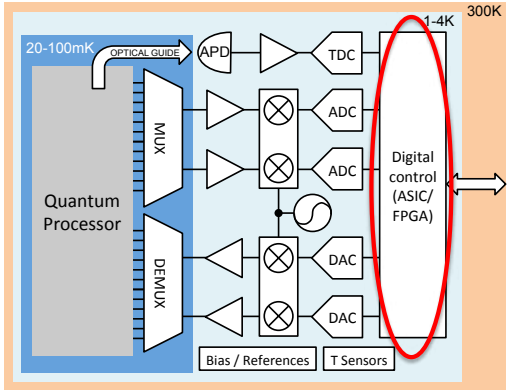

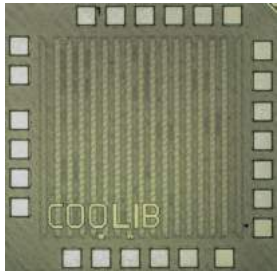

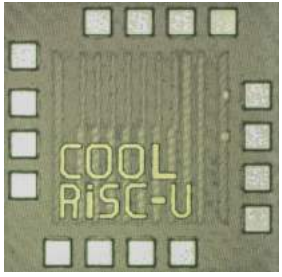

Ultra-Low Voltage Library ‘cooLib’

- Digital library optimized for 4K
- Ultra low voltage operation (100s mV)
- Sub-threshold bias of N/P MOS
- Resilient to latchup and hysteresis-free
- Several logic families (static and dynamic CMOS)
- Compatible with commercial P&R tools

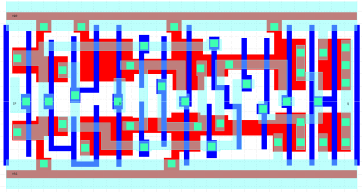

D-Flip-flop optimized for 4K (40nm CMOS)

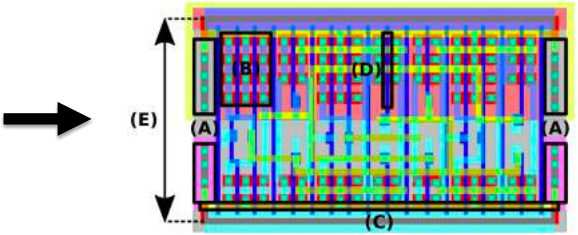

Test Chip Implementation

- Compare ‘CooLib’ cells to foundry supplied std. cells of TSMC40LP process
- Contains commonly encountered digital circuits
  - i.e. unsigned multiplier
- Four versions per circuit
  - Static ‘CooLib’
  - Domino ‘CooLib’
  - TSMC40LP, restricted
  - TSMC40LP, unrestricted
- One ‘true’ domino logic implementation

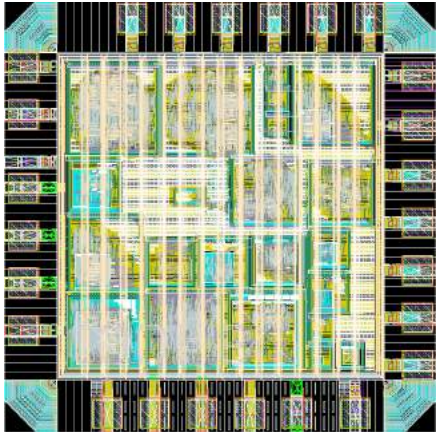

Dynamic vs. Static Power at Cryo

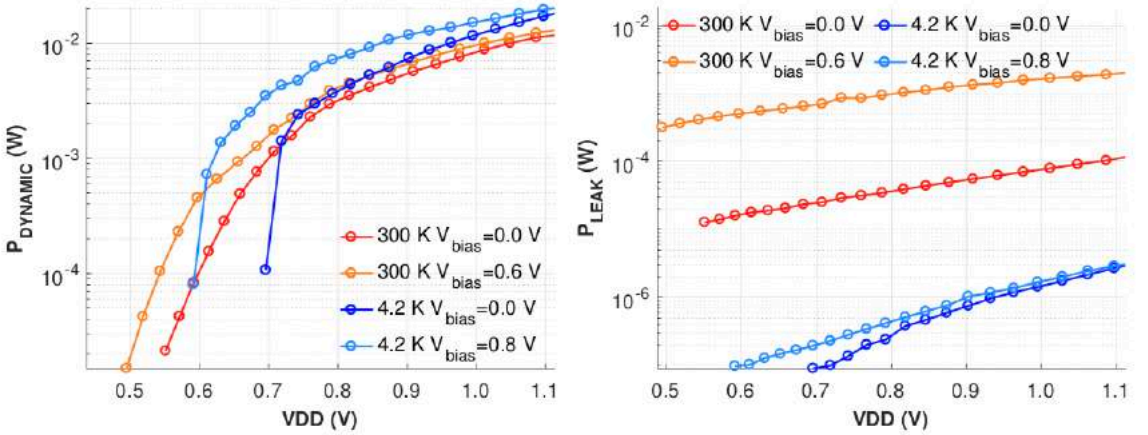

A. Schriek, F. Sebastiano, E. Charbon, *subm*. paper 2020

FOMs

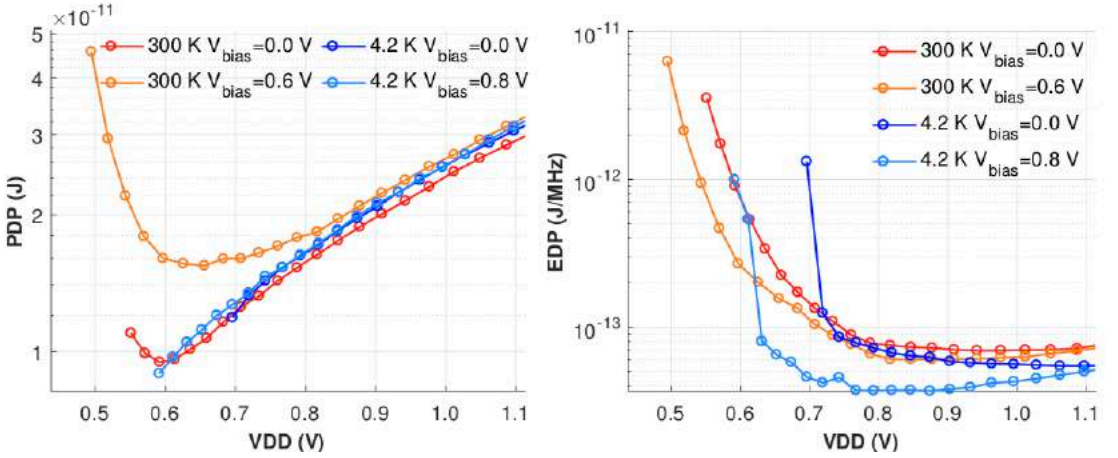

A. Schriek, F. Sebastiano, E. Charbon, *subm*. paper 2020

PDP: power-delay product
EDP: energy-delay product

Benchmarking

		$V_{DD,MIN}$ [V]			F_{MAX} @ 0.6 V [MHz]			F_{MAX} @ 0.7 V [MHz]			P_{AVG} @ 100 kHz [μW]		
Benchmark	Temp.	Pro-posed	A	B	Pro-posed	A	B	Pro-posed	A	B	Pro-posed	A	B
16X16	4.2 K	0.54	0.68	0.68	16.3	-	-	74.2	4.6	2.0	2.34	3.76	3.88
Multiplier	300 K	0.3	0.49	0.44	100.4	9.7	17.4	145.2	34.0	39.7	0.61	2.68	1.92
EPFL	4.2 K	0.58	0.68	0.68	1.95	-	-	20.9	2.2	1.1	3.91	4.00	4.46
Sine	300 K	0.39	0.34	0.39	15.2	9.2	9.5	29.6	25.5	26.4	3.46	2.11	2.18
EPFL Int-to-Float	4.2 K	0.54	0.68	0.68	51.4	-	-	178.1	42.5	11.7	0.80	1.57	3.41
	300 K	0.24	0.38	0.36	118.5	75.2	73.44	174.2	191.9	158.0	0.08	0.55	0.28
EPFL Round-Robin Arbiter	4.2 K	0.58	0.68	0.68	21.6	-	-	46.6	2.0	1.8	7.89	11.56	11.64
	300 K	0.32	0.32	0.31	33.7	10.0	34.7	59.9	37.3	80.8	1.72	3.20	2.25

A. Schriek, F. Sebastiano, E. Charbon, *subm*. paper 2020

‘CooLib’ RISC-V Implementation

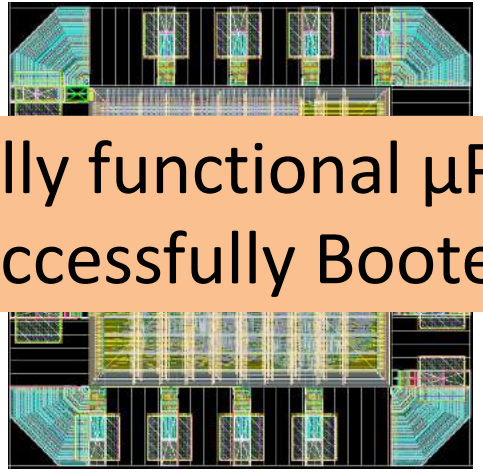

A. Schriek, F. Sebastiano, E. Charbon, *subm*. paper 2020

FEATURES

- RISC-V (picorv32, open-source)
- MC
- UART interface for serial in/output
- JTAG interface for SRAM write/read

Fully functional µP
Successfully Booted LINUX at 4K

Cryo-Single-Photon APDs (Cryo-SPADs)

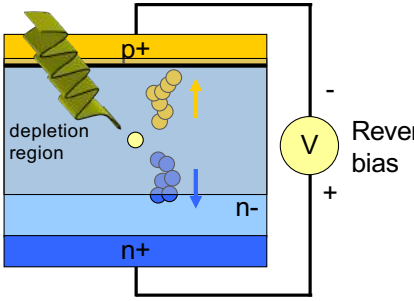

Operation in proportional and Geiger mode (SPAD)

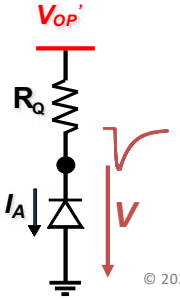

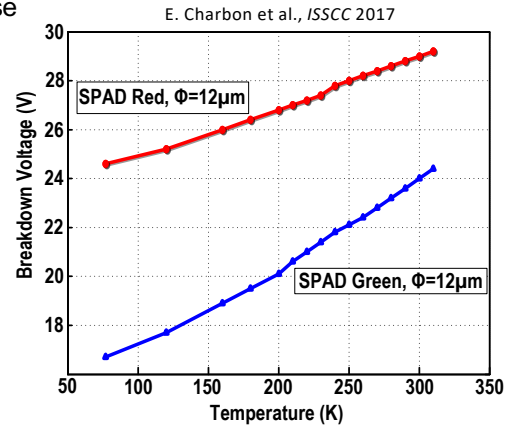

Cryo-SPADs

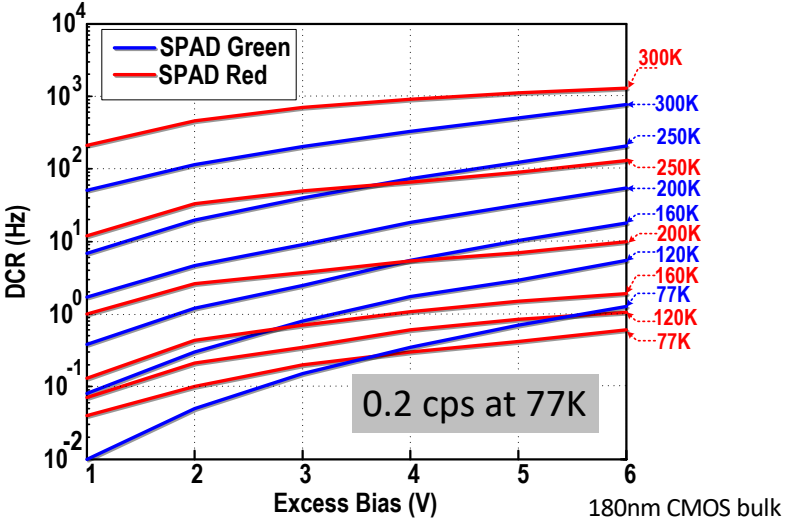

180nm CMOS bulk

B. Patra et al., *JSSC* 2018

Qubits and Control in the Fridge

Step 1: Multiplexing Qubits

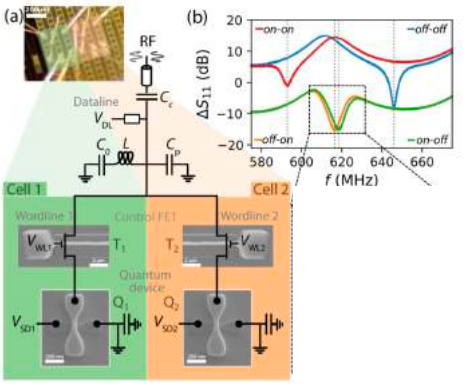

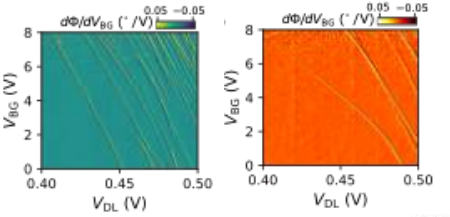

Two device gate maps measured in an interleaved manner

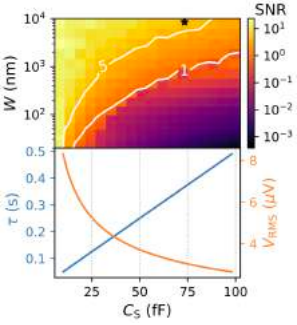

Approach can be applied down to 100nm scale

S Schaal *et al.*, arXiv:1809.03894

Step 2: Reading Qubits

- **Single-shot dispersive readout**
- ***Single electron transistor*** readout
- (limited) use of 3D stacking
- Ideally bring qubits to 1-4K, make them CMOS-compatible

H. Homulle et al., QuRO interface
Silicon Quantum Electronics Workshop, 2018

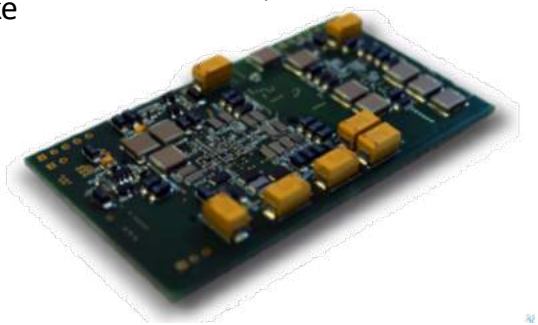

Step 3: Controlling Qubits

- **Lower Speed DAC + Mixer**

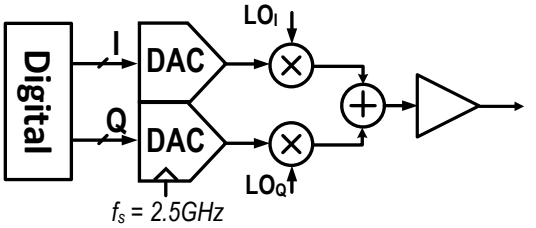

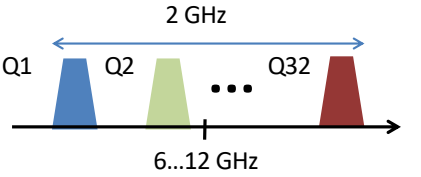

Analog: noise/linearity specifications known + feasible

Controlling Qubits: Specs

- Target fidelity: 99.99% for 1…10 MHz operation

- Analog:

Error Source	*Type*	*Value*	*Contribution*	
Microwave frequency	inaccuracy	35.4 kHz	1-F = 12.5 ppm	
(nominally 5…13 GHz)	noise	35.4 kHz_{rms}	1-F = 12.5 ppm	
Microwave phase	Inaccuracy	0.20 °	1-F = 12.5 ppm	
	noise	0.20 °	1-F = 12.5 ppm	
Microwave amplitude	inaccuracy	38.3 µV	1-F = 12.5 ppm	
(nominally 17 mV, -53 dB)	noise	38.3 μV_{rms}	1-F = 12.5 ppm	
Microwave duration	inaccuracy	113 ps	1-F = 12.5 ppm	
(nominally 50 ns)	noise	113 ps_{rms}	1-F = 12.5 ppm	+
			F = 99.99%	

Controller Architecture: Horse Ridge

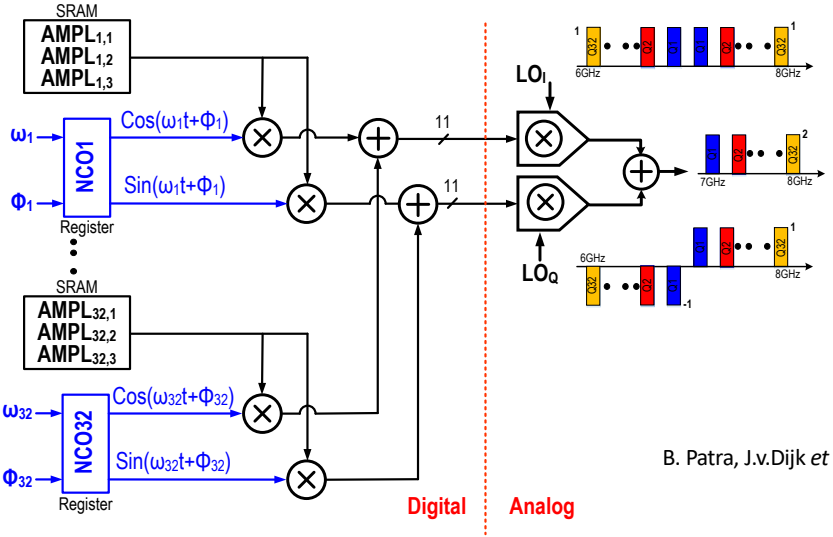

B. Patra, J.v.Dijk *et al.*, *ISSCC* 2020

Controller Implementation

B. Patra, J.v.Dijk *et al.*, *ISSCC* 2020

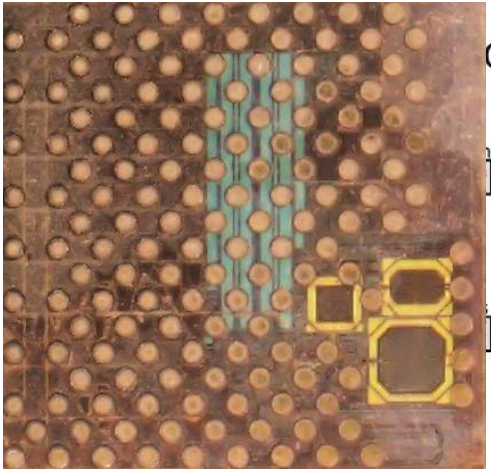

2 mm

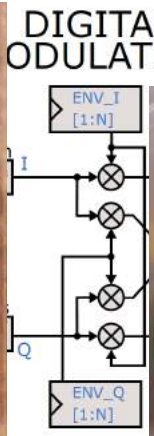

ANALOG
DAC/Filter/Mixer

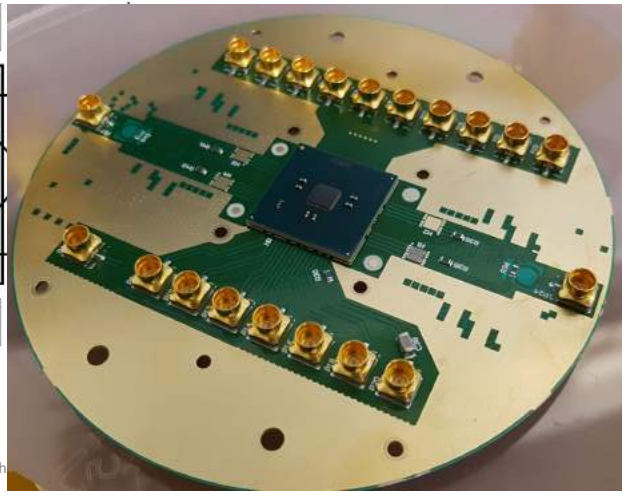

Pulse Shaping

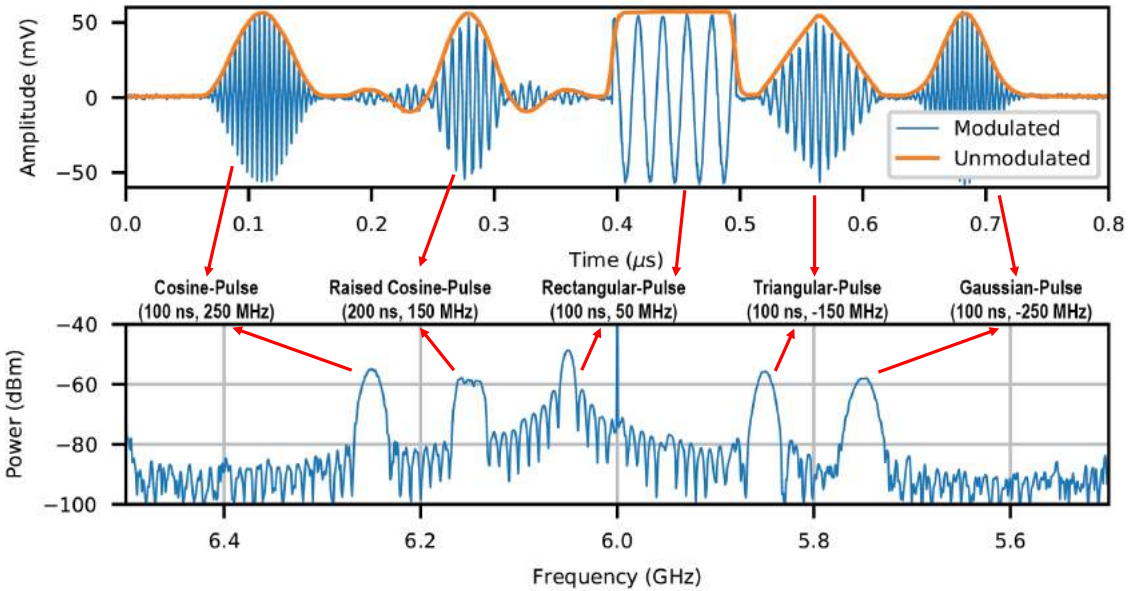

Rabi Experiment

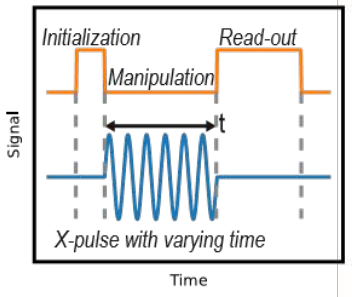

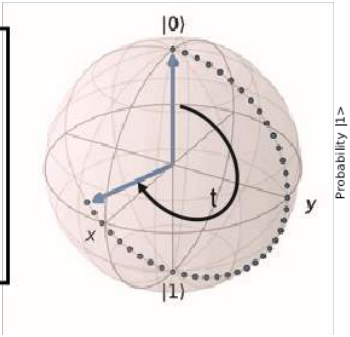

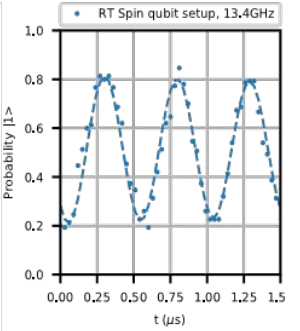

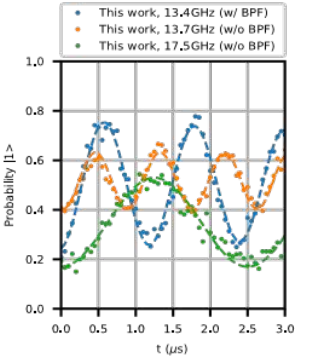

B. Patra, J.v.Dijk *et al.*, *ISSCC* 2020

Qubit Manipulation

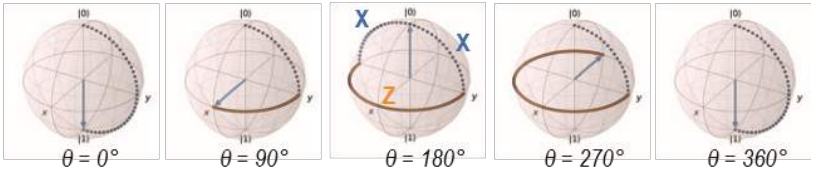

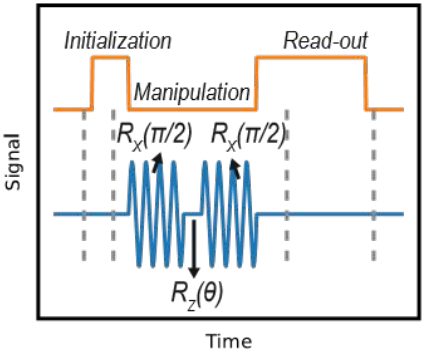

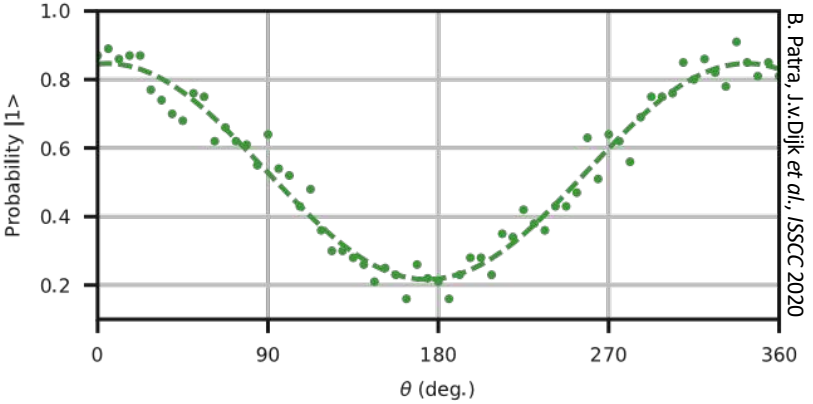

Comparison Table

	Horse Ridge (ISSCC'20)	ISSCC'19	RSI'17	Spin qubit setup
Operating Temperature	3 K	3 K	300 K	300 K
Qubit platform	**Spin qubits + Transmons**	Transmons	Transmons	Spin qubits
Qubit frequency	**2 – 20 GHz**	4 – 8 GHz		< 20 GHz
Channels	**128 (32 per TX)**	1	4	1
FDMA	**Yes, SSB**	No	Yes, SSB	No
Data Bandwidth	1 GHz	400 MHz	960 MHz	520 MHz
Image & LO leakage calibration	**On chip**	Off chip	Yes	
Phase correction	**Yes**	No	No	No
Fidelity (expected)	**99.99%**	-	-	-
Waveform/Instructions	**Upto 40960 pts AWG**	Fixed 22 pts symmetric		16M pts AWG
Instruction set	**Yes**	No	Yes	Yes
Power / TX	Analog: 1.7 mW/qubit * Digital: 330 mW ‡	Analog < 2 mW/qubit # Digital: N/A		850 W
Chip area / TX	4 mm^2	1.6 mm^2	Discrete components	Rack mount
Technology	22 nm FinFET CMOS	28 nm bulk CMOS		

* including LO/Clock driver; only RF-Low active # does not mention circuits included

‡ can be reduced with clock gating

In Summa

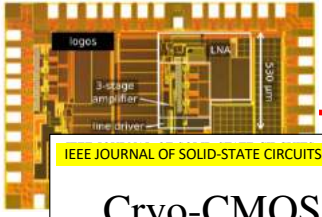

IEEE IEDM 2016

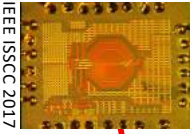

IEEE ISSCC 2017

IEEE IEDM 2016

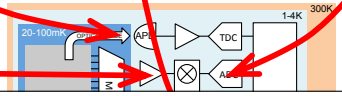

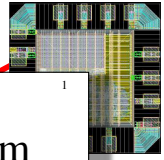

IEEE JOURNAL OF SOLID-STATE CIRCUITS

1

Cryo-CMOS Circuits and Systems for Quantum Computing Applications

Bishnu Patra, *Student Member, IEEE*, Rosario M. Incandela, *Student Member, IEEE*, Jeroen P. G. van Dijk, Harald A. R. Homulle, Lin Song, Mina Shahmohammadi, *Member, IEEE*, Robert Bogdan Staszewski, *Fellow, IEEE*, Andrei Vladimirescu, *Fellow, IEEE*, Masoud Babaie, *Member, IEEE*, Fabio Sebastiano, *Senior Member, IEEE*, and Edoardo Charbon, *Fellow, IEEE*

ISSCC 2020

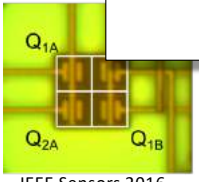

IEEE Sensors 2016

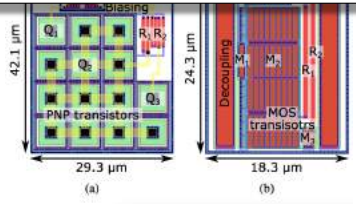

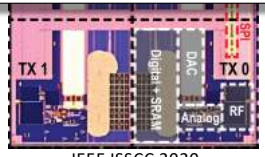

IEEE ISSCC 2020

5. Conclusions

Realizations of 1D Qubit Arrangements

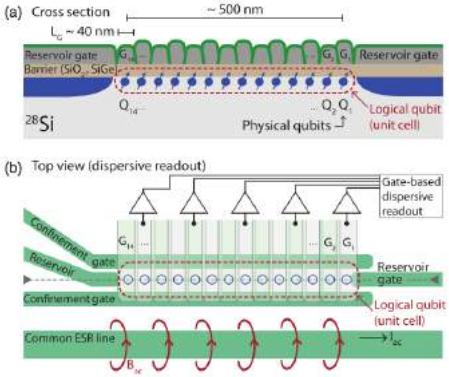

Jones *et al*, PRX 8, 021058 (2018)

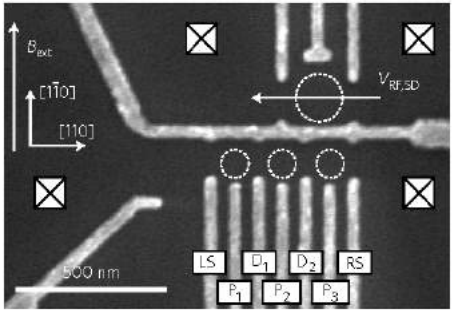

Baart *et al*, Nat Nano (2017)

Proposals for Scalable Fault-Tolerant 2D Qubit Arrangements

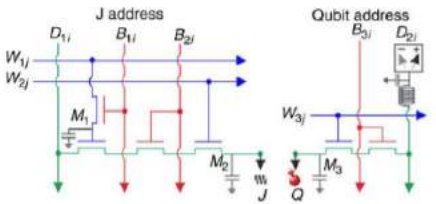

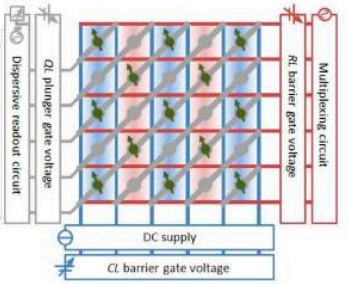

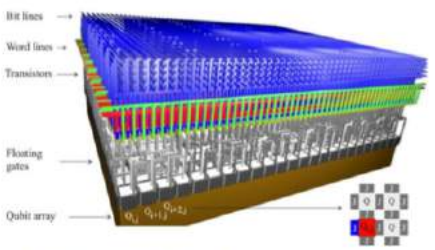

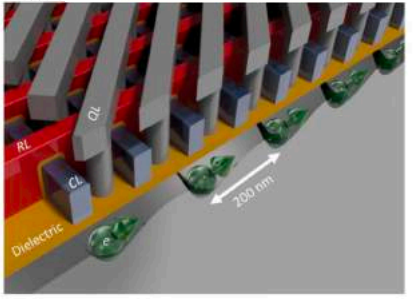

M. Veldhorst *et al.* (UNSW), *Nature Comm.* (2017)

R. Li et al., arXiv 1711.03807 (2017)

SiMOS QD Qubit Operation at 1.5 Kelvin

Silicon quantum processor unit cell operation above one Kelvin

C. H. Yang,[1,*] R. C. C. Leon,[1] J. C. C. Hwang,[1,†] A. Saraiva,[1] T. Tanttu,[1] W. Huang,[1] J. Camirand Lemyre,[2] K. W. Chan,[1,‡] K. Y. Tan,[1,‡] F. E. Hudson,[1] K. M. Itoh,[3] A. Morello,[1] M. Pioro-Ladrière,[2,4] A. Laucht,[1] and A. S. Dzurak[1,§]

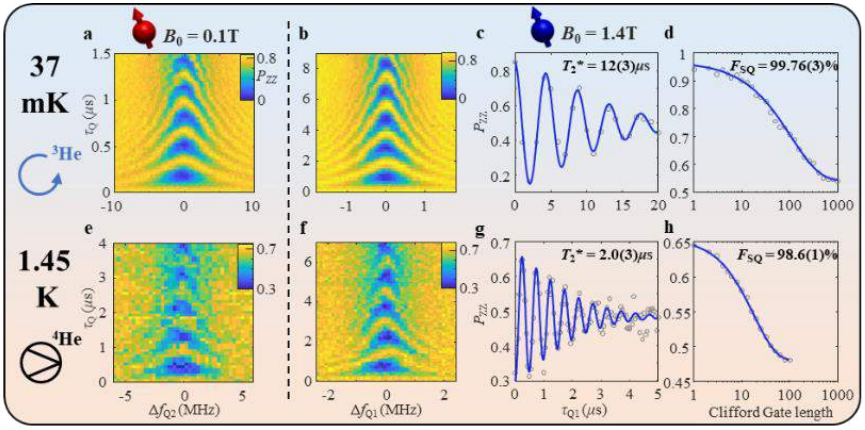

⇒ 1.5 K performance comparable to ^{nat}Si at 100 mK !

Courtesy: A. Dzurak

H. Yang *et al.*, arXiv:1902.09126

UNSW SYDNEY

Platforms for the 2D Approach

- **Single-shot dispersive readout** could be the core of column readouts
- Use ***imaging sensor*** readout as inspiration
- Use tunneling barriers as selectors
- (limited) use of 3D stacking
- Ideally bring qubits to 1-4K, make them CMOS-compatible

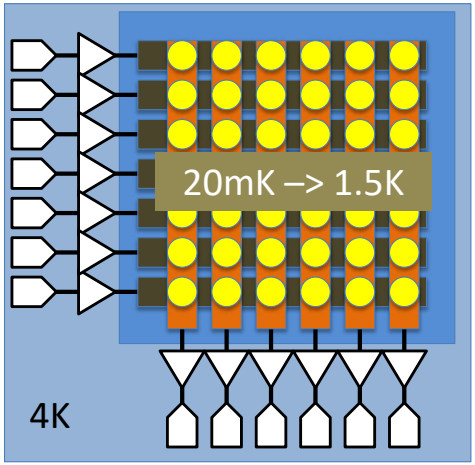

Tradeoffs

1-qubit gate:
Oscillator phase noise
Timing accuracy
…

Fidelity
(99.9%)

2-qubit gate:
Voltage drift
Timing jitter
…

Power
(~ 1 mW/qubit)

Qubit read-out:
Amplitude noise
…

- Fidelity is usually expressed as a percentage, ofter referred to as x9's (e.g. 5 9's = 99.999%)
- Higher fidelity usually requires high power, which is budgeted, espcially at low temperatures (e.g. µW of thermal absorption at mK, while W at 4K)

Quantum Computing

- A quantum computer is a new computing paradigm and as such it holds the promise to handle today's intractable problems
- A qubit is fragile and thus needs to be constantly corrected to extend its coherence and to maintain fidelity
- Cryogenic electronics for quantum computing ensures compactness and scalability to much larger quantum processors

IceQubes: International Workshop on Cryogenic Electronics for Quantum Systems

June 2021, Neuchâtel - Switzerland

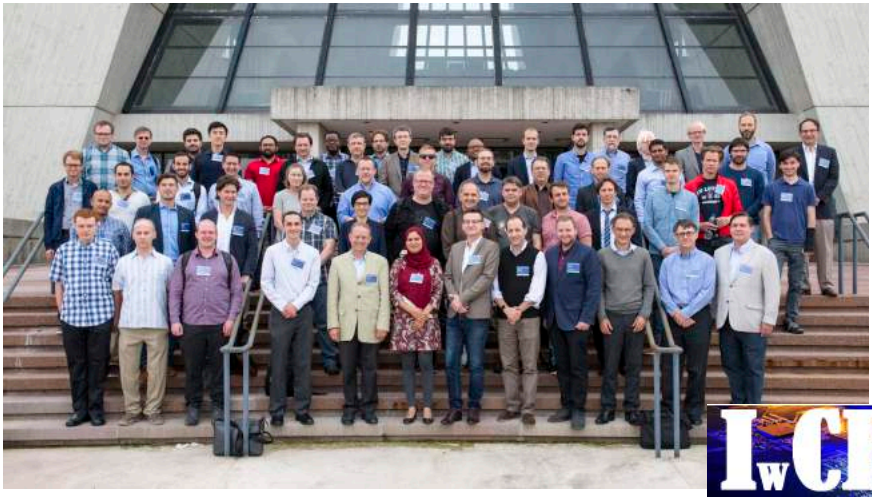

Thank You

http://aqua.epfl.ch

References

- A. Aspect, J. Dalibard, and G. Roger, ‘‘Experimental test of Bell’s inequalities using time-varying analyzers,’’ Phys. Rev. Lett. 49, 1804–1807 (1982).
- D. Wecker, B. Bauer, B. K. Clark, M. B. Hastings, and M. Troyer, Phys. Rev. A 90, 022305 (2014).
- **N.D. Mermin, “Quantum Computer Science: An Introduction,” Cambridge University Press, 5th printing, 2016. ISBN 978-0-521-87658-2**
- **M.A. Nielsen, I.I. Chuang, “Quantum Computation and Quantum Information”, Cambridge Press, 3rd printing, 2017. ISBN 978-1-107-00217-3**
- A. Montanaro, “Quantum Algorithms: an Overview”, npj Quantum Information 2, 15023 EP (2016), review article.
- E. Charbon, F. Sebastiano, A. Vladimirescu, H. Homulle, S. Visser, L. Song, and R. M. Incandela, IEEE International Electron Devices Meeting (IEDM) pp. 13.5.1–13.5.4 (2016).
- H. Ball, W. D. Oliver, and M. J. Biercuk, npj Quantum Information 2, 16033 EP (2016), review article.
- L. Vandersypen, H. Bluhm, J. Clarke, A. Dzurak, R. Ishihara, A. Morello, D. Reilly, L. Schreiber, and M. Veldhorst, arXiv preprint arXiv:1612.05936 (2016).

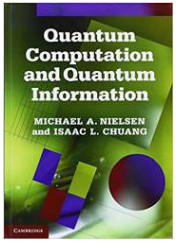

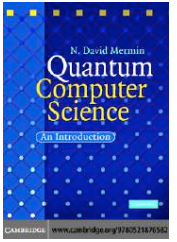

References

- H. Homulle, S. Visser, E. Charbon, “A cryogenic 1 GSa/s, soft-core FPGA ADC for quantum computing applications”, IEEE Transactions on Circuits and Systems I, 63 (11), 1854-1865 (2016).
- H. Homulle, S. Visser, B. Patra, G. Ferrari, E. Prati, C.G. Almudéver, K. Bertels, F. Sebastiano, E. Charbon, “CryoCMOS hardware technology a classical infrastructure for a scalable quantum computer”, ACM International Conference on Computing Frontiers, 282-287 (2016).
- L. Song, H. Homulle, E. Charbon, F. Sebastiano, “Characterization of bipolar transistors for cryogenic temperature sensors in standard CMOS”, IEEE SENSORS, 1-3 (2016).
- F. Sebastiano, H. Homulle, B. Patra, R. Incandela, J. van Dijk, L. Song, M. Babaie, A. Vladimirescu, and E. Charbon, ACM Design Automation Conference (DAC) pp. 13:1–13:6 (2017).
- E. Charbon, F. Sebastiano, M. Babaie, A. Vladimirescu, M. Shahmohammadi, R.B. Staszewski, H. Homulle, B. Patra, J.P.G. Van Dijk, R.M. Incandela, L. Song, B. Valizadehpasha, “Cryo-CMOS circuits and systems for scalable quantum computing”, International Solid-State Circuits Conference (2017).
- H. Homulle, S. Visser, B. Patra, G. Ferrari, E. Prati, F. Sebastiano, E. Charbon, “A reconfigurable cryogenic platform for the classical control of quantum processors”, Review of Scientific Instruments 88 (4), 045103 (2017).
- H. Homulle, E. Charbon, “Performance characterization of Altera and Xilinx 28 nm FPGAs at cryogenic temperatures”, International Conference on Field Programmable Technology (ICFPT), 25-31 (2017).
- D.K.L. Oi, A. Ling, G. Vallone, P. Villoresi, S. Greenland, E. Kerr, M. Macdonald, H. Weinfurter, H. Kuiper, E. Charbon, R. Ursin, “CubeSat quantum communications mission”, EPJ Quantum Technology, 4(1), (2017).

References

- E. Prati, D. Rotta, F. Sebastiano, E. Charbon, “From the Quantum Moore's Law toward Silicon Based Universal Quantum Computing”, IEEE International Conference on Rebooting Computing (ICRC), 1-4 (2017).
- H. Homulle, S. Visser, B. Patra, E. Charbon, ‘’FPGA Design Techniques for Stable Cryogenic Operation’’, arXiv preprint arXiv:1709.04190 (2017).
- R.M. Incandela, L. Song, H. Homulle, F. Sebastiano, E. Charbon, A. Vladimirescu, “Nanometer CMOS characterization and compact modeling at deep-cryogenic temperatures”, 47th European Solid-State Device Research Conference (ESSDERC), 58-61 (2017).
- D. Rotta, F. Sebastiano, E. Charbon, E. Prati, “Quantum information density scaling and qubit operation time constraints of CMOS silicon-based quantum computer architectures”, npj Quantum Information 3 (1), 26 (2017).
- C.G. Almudever, N. Khammassi, L. Hutin, M. Vinet, M. Babaie, F. Sebastiano, E. Charbon, K. Bertels, “Towards a scalable quantum computer”, 13th International Conference on Design & Technology of Integrated Systems In Nanoscale Era (2018).
- H. Homulle, E. Charbon, “Cryogenic low-dropout voltage regulators for stable low-temperature electronics”, Cryogenics 95, 11-17 (2018).
- R.M. Incandela, L. Song, H. Homulle, E. Charbon, A. Vladimirescu, F. Sebastiano, “Characterization and Compact Modeling of Nanometer CMOS Transistors at Deep-Cryogenic Temperatures”, IEEE Journal of the Electron Devices Society (2018). Doi: 10.1109/JEDS.2018.2821763.

References

- JPG van Dijk, A Vladimirescu, M Babaie, E Charbon, F Sebastiano, “A co-design methodology for scalable quantum processors and their classical electronic interface”, Design, Automation & Test in Europe Conference (2018).
- JPG van Dijk, E Kawakami, RN Schouten, M Veldhorst, LMK Vandersypen, M Babaie, E Charbon, F Sebastiano, “The impact of classical control electronics on qubit fidelity”, arXiv:1803.06176 (2018).
- H Homulle, L Song, E Charbon, F Sebastiano, “The Cryogenic Temperature Behavior of Bipolar, MOS, and DTMOS Transistors in Standard CMOS”, IEEE Journal of the Electron Devices Society 6 (1), 263-270 (2018).
- H. Homulle, F. Sebastiano, E. Charbon, “Deep-Cryogenic Voltage References in 40-nm CMOS”, IEEE Solid-State Circuits Letters, 1(5), 110-113 (2018). Doi: 10.1109/LSSC.2018.2875821.
- B. Patra, R.M. Incandela, J. P. G. van Dijk, H. A. R. Homulle, L. Song, M. Shahmohammadi, R. B. Staszewski, A. Vladimirescu, M. Babaie, F. Sebastiano, and E. Charbon, “Cryo-CMOS Circuits and Systems for Quantum Computing Applications”, IEEE Journal of Solid-State Circuits, 53(1), 309-321 (2018).
- J.P.G. van Dijk, E Charbon, F Sebastiano, “The electronic interface for quantum processors”, Microprocessors and Microsystems, Jan. 2019.
- J.P.G. van Dijk, E. Kawakami, R.N. Schouten, M. Veldhorst, L.M.K. Vandersypen, M. Babaie, E. Charbon, and F. Sebastiano, “Impact of Classical Control Electronics on Qubit Fidelity”, Physical Review Applied, 12, 044054 (2019). Doi: 10.1103/PhysRevApplied.12.044054.

References

- M. Mehrpoo, F. Sebastiano, E. Charbon, M. Babaie, “A Cryogenic CMOS Parametric Amplifier”, IEEE Solid-State Circuits Letters, 3, 5-8 (2019). Doi: 10.1109/LSSC.2019.2950186.
- B. Patra, M. Mehrpoo, A. Ruffino, F. Sebastiano, E. Charbon, M. Babaie, “Characterization and Analysis of On-Chip Microwave Passive Components at Cryogenic Temperatures”, IEEE Journal of the Electron Devices Society, 8, 448-456 (2020). Doi: 10.1109/JEDS.2020.2986722.
- P. ‘t Hart, M. Babaie, E. Charbon, A. Vladimirescu, F. Sebastiano, “Subthreshold Mismatch in Nanometer CMOS at Cryogenic Temperatures”, IEEE Journal of the Electron Devices Society, X(X), XXX-XXX, (2020). Doi: 10.1109/JEDS.2020.2988730.
- A. Ruffino, Y. Peng, F. Sebastiano, M. Babaie, E. Charbon, “A Wideband Low-Power Cryogenic CMOS Circulator for Quantum Applications”, IEEE Journal of Solid-State Circuits, 55(5), 1224-1238 (2020). Doi: 10.1109/JSSC.2020.2978020.
- T.-Y. Yang, A. Ruffino, J. Michniewicz, Y. Peng, E. Charbon, M. Gonzalez-Zalba, "Quantum Transport in 40-nm MOSFETs at Deep-Cryogenic Temperatures", X(X), XXX-XXX, IEEE Electron Device Letters (2020). Doi: 10.1109/LED.2020.2995645.
- A. Stanco, D.G. Marangon, G. Vallone, S. Burri, E. Charbon, P. Villoresi, “Efficient random number generation techniques for CMOS single-photon avalanche diode array exploiting fast time tagging units”, to appear, APS Physical Review Research, 2, 023287 (2020). Doi: 10.1103/PhysRevResearch.2.023287.
- P. ‘t Hart, M. Babaie, E. Charbon, A. Vladimirescu, F. Sebastiano, “Characterization and Modeling of Mismatch in Cryo-CMOS”, IEEE Journal of the Electron Devices Society, 8(1), 263-273 (2020). Doi: 10.1109/JEDS.2020.2976546.